Alma Mater Studiorum - Università di Bologna

SCUOLA DI SCIENZE

Dipartimento di Chimica Industriale “Toso Montanari”

Corso di Laurea Magistrale in

Chimica Industriale

Classe LM-71 - Scienze e Tecnologie della Chimica Industriale

Pt-Cu catalytic coatings for hydrogen combustion: nanostructure and dealloying effects

Tesi di laurea sperimentale

CANDIDATO

Francesco Giarratano

RELATORE

Chiar.mo Prof. Maria Cristina Cassani

CORRELATORE

Chiar.mo Prof. Asunción Fernández

Dott.ssa Vanda Godinho

Dott.ssa Gisela M. Arzac

Anno Accademico 2015-2016

ABSTRACT

This thesis work was carried out at Materials Science Institute of Seville, ICMS (Spain). CSIC-Univ.Seville, at the group of nanotechnology, under the supervision of the Prof. Maria Asunción Fernández. The aim of this thesis was to synthesize and characterize supported thin films of metallic nanocatalysts (Pt-Cu) supported on silicon carbide. The nanocatalysts have been produced by a physical vapor deposition (PVD) technique, precisely the magnetron sputtering.

One of several possible techniques to check and modify the reactivity of nanocatalysts is the dealloying. The selective leaching in an acid environment was used on nanocatalysts in this thesis. The supported metal alloys produced have been chosen to test on the reaction of Catalytic Hydrogen Combustion (CHC). The work was therefore divided into two parts.

- In the first the synthesis of the supported metal alloy has been developed, through the use of magnetron sputtering;
- the second step was the use of the technique of dealloying in acidic environment;
- the third step was the characterization of the of produced coatings. Through spectroscopic techniques XRD, SEM and EDX.

➢ In the second part a process for the CHC reaction on supported nanocatalysts coatings has been developed;

➢ after testing the samples, the reported results were used to calculate the activation energy of the reaction CHC and the T_{50}.

Index

1-Introduction 5

1.1 Nanotechnology and nanomaterials 5

1.2 Sputtering deposition 6

1.3 Magnetron sputtering 8

1.4 Structure and properties of thin films 14

1.5 Dealloying of Noble-Metal alloys 16

1.6 Substrate 20

1.7 Aim of the thesis 21

2- Characterization methods 22

2.1 Scanning electron microscope (SEM) 22

2.2 Energy Dispersive X-rays spectroscopy (EDX) 24

2.3 X-ray diffraction (XRD) 25

3-Description of the magnetron sputtering system 33

3.1 Characterization with XRD 34

3.2 Pt-Cu coatings: microstructural characterization by SEM 36

3.3 Pt-Cu coatings under Helium: microstructural characterization by SEM 36

3.4 Pt-Cu coatings under Argon: microstructural characterization by SEM 39

3.5 Pt-Cu coatings: Microstructural characterization by EDX 43

3.6 Conclusion 47

3.7 Catalytic hydrogen combustion CHC 48

3.8 Catalytic tests results 50

3.9 Conclusion 55

3.10 Experimental part 56

3.10.1-Synthesis of copper platinum alloys by magnetron sputtering and subsequent treatment of dealloying 56

3.10.2- Support and catalyst characterization SEM 58

3.10.3- Catalytic tests 58

4-Conclusions 61

References 62

1– INTRODUCTION

1.1 Nanotechnology and nanomaterials

Nanotechnology relies on the ability to design, manipulate, and manufacture materials at the nanoscale (between 1 nanometer and 100 nm in size). The nanoscale is the scale of atoms and molecules, the fundamental building blocks of the material world. At the nanoscale, scientists can start affecting the properties of materials directly, making them harder or lighter or more durable. In some cases, simply making things smaller changes their properties (a chemical might take on a new color, or start to conduct electricity when re-fashioned at the nanoscale). These materials are called nanomaterials [1].

Commercial processes and products that use nanomaterials are growing rapidly and these tiny products are increasingly found in paint, fabrics, cosmetics, treated wood, electronics and sunscreen. Nanomaterials exhibit unique properties different than chemical substances that are larger in size, because they have more surface area. In the chemistry sector, nanomaterials are used as catalyst for various industrial processes, for environmental monitoring (membranes, devices), and for different applications in the manufacturing industry (construction and active materials for the packaging). Nanomaterials provide opportunities for the development of innovative products that provide advances in technologies and medicine [2].

The ultimate goal in catalytic design is to have complete synthetic control of the material properties that determine the reactivity. Catalysts that consist of two metals (bimetallic) allow greater reactivity and more flexible design, and recent studies have focused on these catalysts. This thesis work has had as its object the production and characterization of thin films of copper and platinum by magnetron sputtering, with subsequent catalytic test. The study of thin film involves several research fields, in which fall, chemistry, engineering, and science of materials. In recent years this branch of technology is experiencing a rapid growth.

Among the methods of creation of the thin films, the sputtering technique plays an important role because it turns out to be versatile, relatively fast and economically efficient. In this thesis the technique of magnetron sputtering is described, it was adopted for the deposition of thin films of copper and platinum. Films were deposited by the magnetron sputtering technique on substrates of silicon carbide. The characterization was based on a measurement of their thickness, also in order to define the degree of uniformity of the deposit obtained with the used magnetron sputtering, and subsequently

in an analysis of their internal structure. The surface properties of these films are significant and they are influenced by different conditions of film deposition. The most important are: temperature, pressure and the material to be coated.

The catalytic part included a point where the structure of the film is modified by the technique of dealloying. The effects of the nanostructure induced by the magnetron and the porosity caused by the dealloying were tested by the Catalytic Combustion of Hydrogen (CHC), an important reaction in the hydrogen economy, which can be employed as a means of heat production as well as for safety purpose.

1.2 Sputtering deposition

This paragraph will be dedicated to present an overview on the deposition technique used to prepare the coatings presented in this thesis.

Sputtering deposition is a physical vapor deposition technique in which a target is bombarded with energetic ions provoking the ejection of the atoms from the target that are finally deposited on a substrate forming a layer. This most common form of sputtering is a plasma-based sputtering. The plasma is formed by the partial ionization of a gas applying an electric discharge between the target (cathode) and the substrate to be covered (anode).

In Fig.1 the sputtering process is sketched showing the different components of the plasma: ions, electrons, neutral atoms and photons. These last ones give the color to the plasma. When the energy of the formed ions is high enough, the interaction with the target surface creates a collision cascade and some of the momentum is transferred to the surface atoms which can be ejected – sputtered.

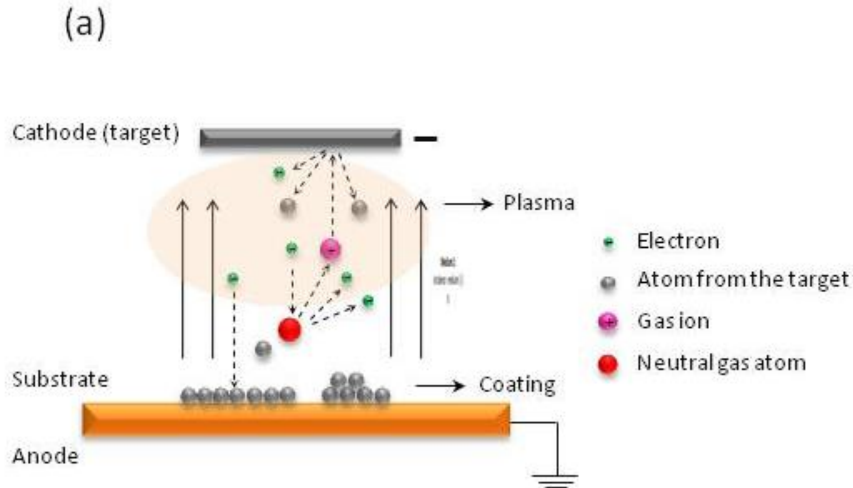

Fig.1 The sputtering process.

These ejected atoms travel some distance until reaching the substrate and condensate forming a thin film. Most of the transferred energy appears as heat in the target surface and near surface. Generally in sputtering the targets are actively cooled, minimizing the radiant heat and preventing also diffusion processes in case of alloy compounds.

Fig.2 presents some of the most significant events that occur on a bombarded target. In addition to the ejection of the atoms, some of the bombarding ions are reflected as high energy particles and some are implanted on the surface.

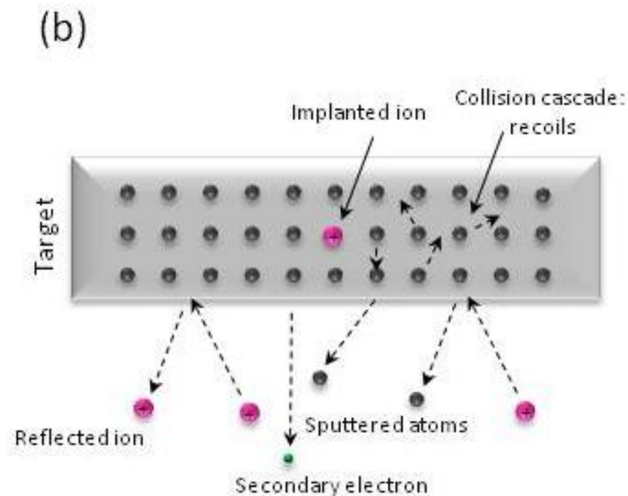

Fig.2 The bombarded target.

Ejected secondary electrons also can interact with the gas atoms through inelastic collisions increasing the ionization probability and creating more ions necessary to sustain the plasma [5].

The number of sputtered atoms depends on the energy, mass and incident angle of the bombarding ion on the target, and also on the target material, its surface binding energy and crystallographic orientation. The sputtered atoms travel through the plasma in vapor phase and when they arrive to the substrate they condensate and are deposited.

Possible ways to increase the ionization probability are by one hand to increase the number of gas atoms increasing the gas pressure or to increase the applied potential. However these measures have some disadvantages. The deposition rate is reduced at higher gas pressure by ion-electron recombination and sputtered atoms collisions in the gas phase, producing also poor quality of the film. Increased potential will also increase energy consumption.

1.3 Magnetron sputtering

In conventional sputtering, the electrons that are ejected from the cathode are accelerated away from the cathode and not all are efficiently used for sustaining the discharge. A good solution to improve deposition process is the use of an adequate magnetic field, deflecting the secondary electrons to keep them near the target surface. The confinement of electrons causes that the same electron participates in ionization events several times increasing the number of ions created and therefore the number of sputtered atoms and secondary electrons by the impact on the target. These secondary electrons would be trapped by the magnetic field and so on. This configuration, named magnetron sputtering, allows generating stable plasma with high density of ions, increasing the deposition rate.

Fig.3 shows a representation of the magnetron sputtering process as it has been used in this thesis for the fabrication of thin films.

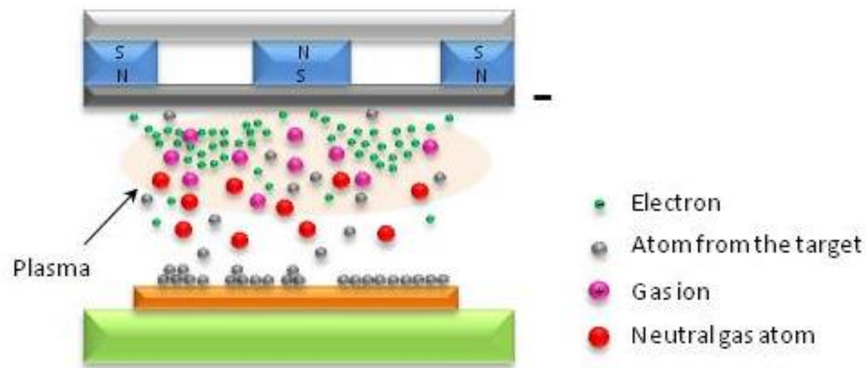

Fig.3 The magnetron sputtering process.

The most common magnetron configuration is the planar magnetron source, where the sputter-erosion path is a closed circle on a flat target denominated "race track". Fig.4 shows the magnet configuration and a representation of the magnetic field lines and their intensity for the magnetron source used in this thesis.

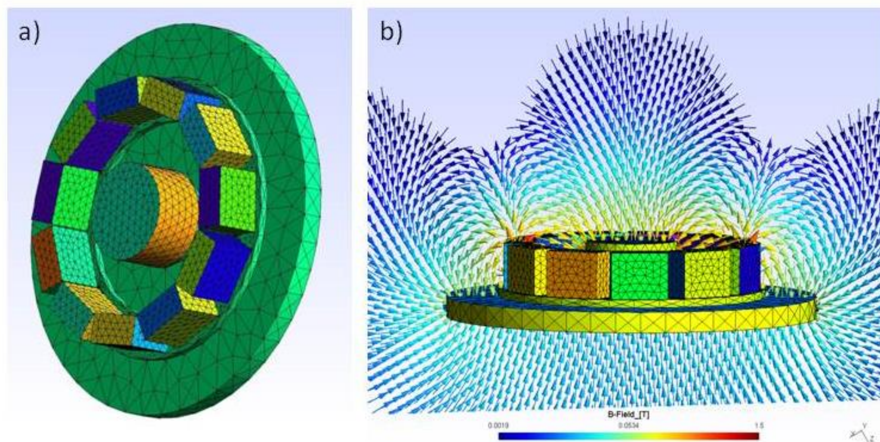

Fig.4: (a) Magnet position and (b) Magnetic field lines and its intensity for the magnetron source used in this thesis (2" magnetron from Thin Film Consulting). Courtesy of Romain Tonneau (university of Namur, Belgium) based on magnetic field measurements carried out in Seville using a magnetic field probe.

Two magnet configurations are also possible depending on the magnets strength. In balanced magnet configuration, the one used in this work as shown in Fig.5(a), the magnets strength and dimensions are the same resulting in strongly confined plasma near

the target region. Therefore, only a few charged particles reach the substrate. This prevents the bombardment of the substrate by energetic particles.

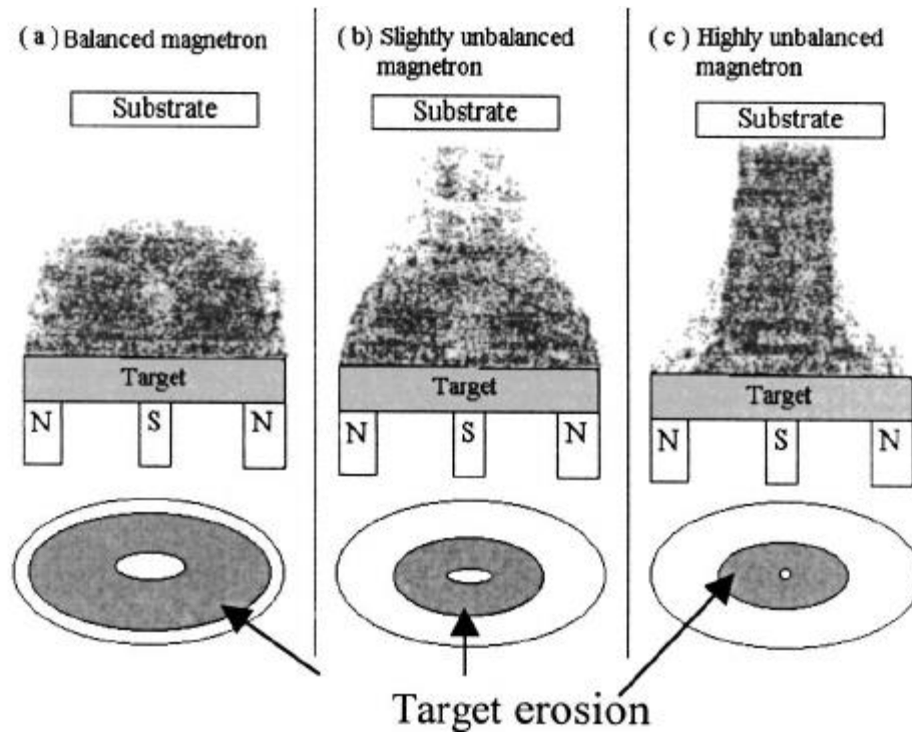

Fig.5 Possible magnetron sputtering configurations.

However, the plasma confinement near the target can be detrimental in activating reactive gases in reactive sputtering deposition, or in situations where it is advantageous to deliver more energy to the substrates. In these situations unbalanced magnet configuration is used, being possible to use magnets with different strength and/or dimensions increasing the plasma's density near to the substrate [4].

External bias voltage can be applied to the substrate in order to increase the particles' energy towards the substrate. If a negative bias is applied, the ions are attracted to the substrate and the electrons repelled, while a positive bias has the opposite effect. Biased coatings are generally denser when compared to the typical columnar growth of non-biased films. It is worth to mention that magnetron sputtering configuration has a drawback related with the irregular erosion of the target. The plasma's density is higher where the magnetic field lines are parallel to the target, so, in this area, the "race track" is formed wasting the target. This may affect the film uniformity and requires frequent replacement of the target. To improve target utilization, rotating cylindrical magnetrons, employing cylindrical tubular targets have been developed [4].

Commonly sputtering deposition occurs in the presence of inert gases like argon or helium, this is the case of the coatings deposited during this thesis. When a reactive gas (as nitrogen or oxygen) is added to the discharge it is possible to deposit a broad variety of compound materials, controlling the composition of the coatings. This is called reactive sputtering. However, the introduction of a reactive gas in contact with the target leads to the formation of compound material poisoning the target's surface, usually with sputtering rates lower than the one of the pure target [3].

There are several modes of powering magnetrons: direct current (DC), radio frequency (RF), and recently high-power impulse magnetron sputtering (HIPIMS). The direct current (DC) mode is the simplest and least expensive and has been applied successfully in metallic targets. However, for semiconductor or insulating targets, this mode fails, due to the accumulation of positive charge on the target interrupting the sputtering process and producing strong arcing. Besides, only a small fraction of the gas is converted to ions resulting in a low deposition rate, so, high gas pressure is necessary to increase the deposition rate this affecting the film quality.

A solution to these problems is to apply a voltage variable with the time with a frequency ω. If the polarity of the target is changed with the time the positive charge accumulation on the target is avoided. This is the named alternate current (AC) sputtering mode. At low frequency ω, the electrons and ions can follow the variation of electric field, and it would be as a DC mode, sputtering the target with electrons or with ions depending of the polarity of the target in every instant. At high frequencies, when the alternating signal is applied to the cathode, generating plasma, then the plasma acts as a rectifier that generates an average negative voltage at the smaller of both electrodes, which is in general the target. This negative voltage is called the self-bias. Due to the different masses, electrons can react to the variation of electric field, while ions are too heavy are only affected by the self-bias voltage Vsb that accelerates them to the target. In Fig.6 is represented a typical voltage variation with the time in AC mode at high frequencies.

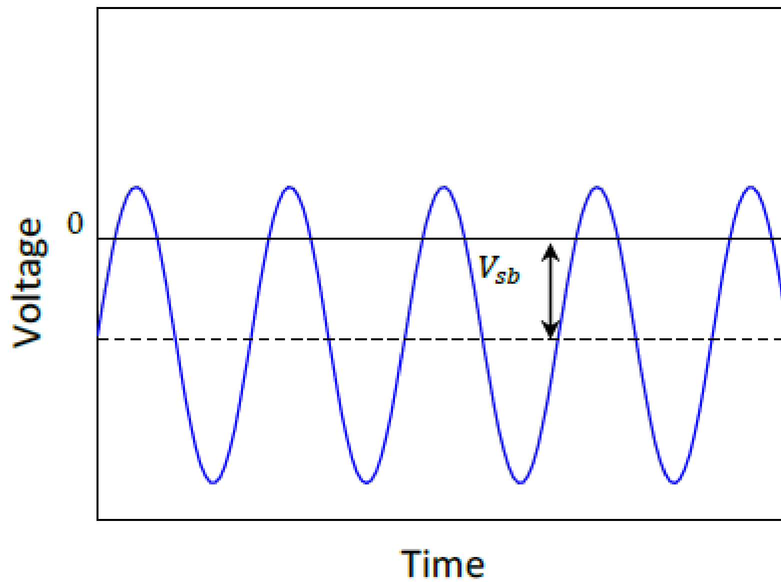

Fig.6 AC voltage on the target and self-bias Vsb.

Usually, the frequency value used is 13.56 MHz in the radiofrequency range. The AC mode in this range is named radiofrequency (RF) mode. RF mode has been employed in this thesis.

So, in the case of RF mode, the electrons are oscillating back and forth colliding more times with the gas atoms before they are lost, and therefore, increasing the ionization degree compared with the DC mode. This means that it is possible to work with lower gas pressure increasing the deposition rate because there are less collisions between the sputtered atoms and the gas atoms. Since the target is capacitive connected to the plasma it makes no difference whether the target is of conductive or electrically isolating material. In spite of these advantages for RF mode in many industrial applications the DC mode is preferred for its easier up-scaling.

HIPIMS uses a large energy impulse on a very short period, typically 100 μs. This method results in high density plasma with a high ionization degree of the sputtered material [4].

Compound materials can also be prepared by the use of alloy targets or co-deposition from different targets. For practical purposes a single target arrangement was used which reduces the consumption of platinum; after calculating the area required to be covered to reach the desired composition; on the copper target fifteen platinum strips were attacked with the aid of copper scotch tape. The target material has been used as scotch tape, in order to avoid interference during sputtering. Fig.7 shows the target used after the application of platinum strips

Fig.7 Copper target after having bonded platinum strips.

Before introducing the process gas, which must then be ionized, it is necessary to get into the environment of deposition at very high vacuum conditions, in order to avoid contaminating the environment itself with the gases present in the air. The vacuum in the sputtering chamber should be created through the combination of at least 2 pumps. It is necessary to first reach a certain level of pressure (of the order of 10^{-3} mbar) in the chamber using a mechanical rotary pump, which extracts the majority of air molecules present, and only then will be filled by a pump able to achieve more vacuum conditions (typically with pressures around 10^{-7} mbar); for this purpose it lends itself well a turbomolecular pump (this configuration was adopted for the deposition object of this thesis): in this type of pump the rotor part can reach very high speeds (1000 rpm / second) and imparts to the particles of a given time a gas. Given the high speeds involved, this type of machine requires a very precise design from the mechanical point of view, in which one must minimize friction to a minimum. It should also not work in the presence of abrasive particles or in conditions of "not empty" (which justifies the preventive action of a rotary pump), as this would lead to its damage. The part of the pump facing the inside of the deposition chamber must obviously be protected by a screen so that it does not become the object of deposition.

Magnetron sputtering presents important advantages over other deposition processes, among them, the possibility of depositing films in a wide variety of substrates even substrates sensible to temperature like polymers, the sputtering conditions can be easily reproduced from run to run. It is a low cost process without the need of chemical precursors avoiding toxic emissions of by-products. One of the major advantages of the magnetron sputtering process is the easiness to scale up to industrial processes.

1.4- Structure and properties of thin films

During deposition the film grows through the condensation of atoms that result to be movable on the substrate surface. The factors that influence the growth and the properties of the film are:

- condition of the substrate surface (morphology, chemical composition, stability, imperfections, gas emissions, preferential nucleation areas);
- characteristics of the deposition process (angle of incidence, distribution of adatomic flow (a flow of adsorbed atoms), substrate temperature, deposition rate, gaseous contaminations);
- reactions and post-deposition processes (reactions of the film surface with the environment, thermal and mechanical cycles, corrosion, deformation).

Moreover a certain homogeneity of the surface to be coated allows to have in turn a certain uniformity of the properties of the film along it, while its morphology has effect on the angle of incidence of the adatomic flow in specific areas, for example by conditioning the development of a type columnar inside the structure.

As already said the preparation of the surface for the deposit has also effect on the characteristics of the film that will be born on it, indeed its purpose is to create a surface as homogeneous as possible by ensuring that the same surface is not changed in an undesirable manner during the preparation.

Generally as the film grows, the roughness of its surface area increases, as some crystallographic planes grow faster than others.

The films deposited atomically generally have a consistent morphology lined trunks, called columnar growth morphology, as shown in Fig.8. It develops for "geometric effect" and can be found both in crystalline materials, both in amorphous materials, in that it is a function of the geometry of the surface, the angle of incidence of the adatomic flow and surface mobility of adatoms same. It should be noted that the columns are not single crystal grains.

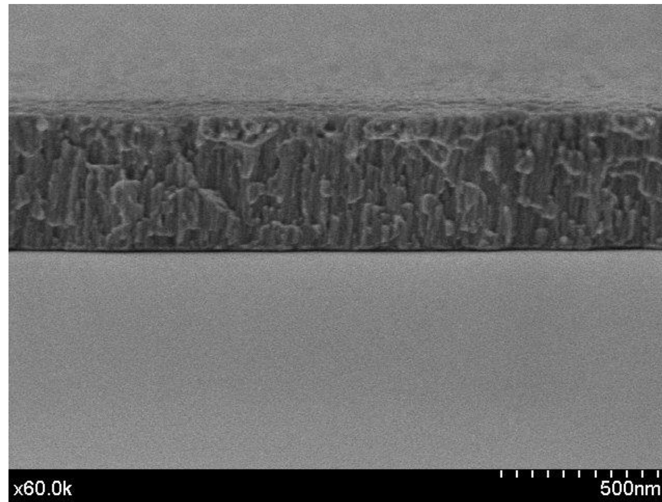

*Fig.8 Example of columnar growth deposited on silicon at the pressure of 4.8 * 10^{-2}mbar, with a discharge voltage of 100 V.*

The columnar development begins to occur quite early in the film growth process and generally becomes prominent after about 100 nm thick. The growth process of the film on the substrate can be divided several stages:

- The adatoms (atoms that lies on a crystal surface) from the target impact the surface of the substrate, after the impact lose their speed component. Initially the adatoms are not in thermal equilibrium with the substrate and tend to move on its surface; during this phase they interact with each other forming larger clusters;
- clusters are thermodynamically unstable and tend to desorb over time. If the deposition parameters are such as to ensure that the clusters are in contact with other before being desorbed, they can grow in size. Once they reach a certain critical mass the clusters become stable thermodynamically. This phase is called the nucleation. The various cores grow until it gets to a certain saturation density; growth can take place parallel to the surface of the substrate (for diffusion of the adatoms) or perpendicular. The nuclei grown at this stage of the process giving rise to islands;
- then the coalescence phase start, in which the islands tend to stick to each other to form larger islands; this phenomenon can be favored by increasing the surface mobility of the particles, for example by increasing the substrate temperature.

1.5- Dealloying of Noble-Metal alloys

Noble-Metal alloys are of high interest specially for catalytic purposes. Dealloying technology is one of the most effective methods for the fabrication of nanostructured materials. Dealloying is currently used to tailor the morphology and composition of nanoparticles and bulk solids for a variety of applications including catalysis related to energy storage, transport and conversion.

For designing and controlling active catalysts, a fundamental understanding of the relationship between the activity and the surface electronic structure and surface chemistry is actively being pursued. Selective leaching, also called dealloying, or selective corrosion, is a corrosion type in some solid solution alloys, when in suitable conditions a component of the alloys is preferentially leached from the material. The figure shows the starting material (a); after the dealloying technique (b); after a prolonged exposure to the selective leaching (c). Each one of these modifications has been reported to yield a considerable enhancement in catalytic activity. This process is an important pathway to create noble metal surface overlayers. The less-noble metal tends to dissolve from the alloy in the acidic media provided by the membrane, the Fig.11 shows that dealloyed Pt-Cu thin films consist of a Pt enriched surface layer and Cu depleted interior and that the Pt surface layer is compressively strained [6].

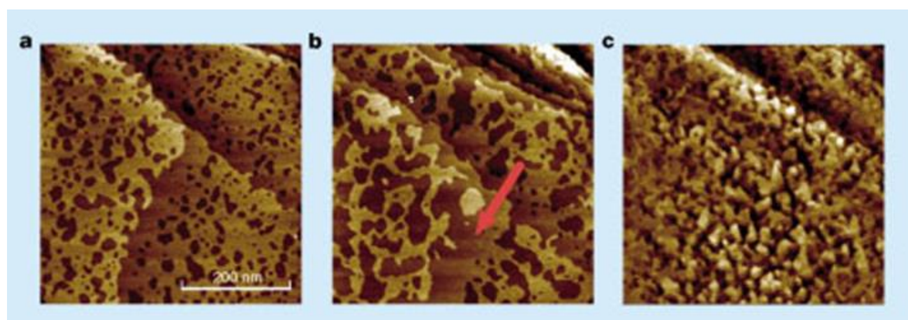

Fig.9 The early stages of dealloying of a copper-gold immersed in a solution of sulfuric acid.

Regarding the morphology from previous studies in the literature is known that dealloying of nanoparticles, include core–shell, hollow core–shell, and porous nanoparticles. The core-shell structure is shown in Fig.10.

In literature after dealloying the PtCu alloy shows nanoparticles with core-shell structure for a size range (2-6 nm)..

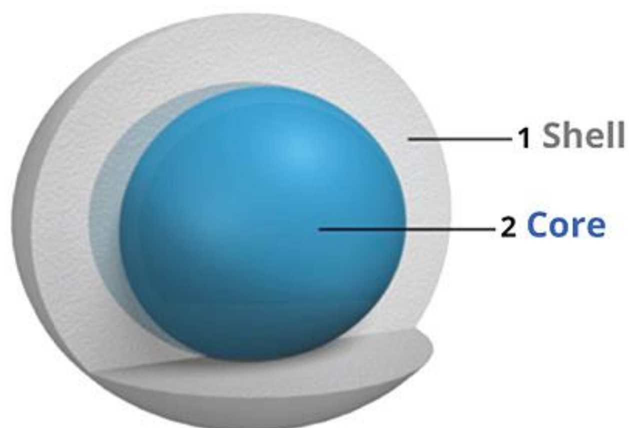

Fig.10 Core-shell particle.

The lattice strain in the Pt shell is most relevant for surface catalysis. The lattice mismatch between the Pt shell and the Pt-Cu core causes a reduced Pt–Pt interatomic distance in the shell. The richer in Cu the particle core, the smaller its lattice parameter, and hence the more strain induced in the shell. This enrichment on the surface is shown in Fig.11.

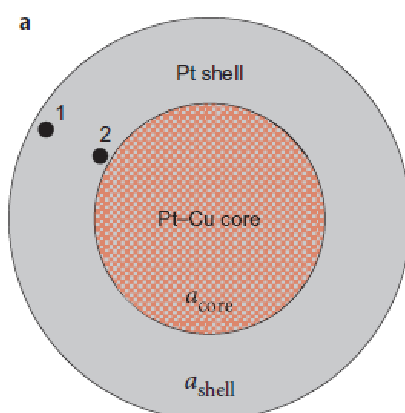

Fig.11 PtCu core-shell structure.

Pure Pt layers surround an alloy particle core is shows in Fig.12a. Increasing the size of the nanoparticles up to (20-55 nm), after the dealloying a porous structure has been found.

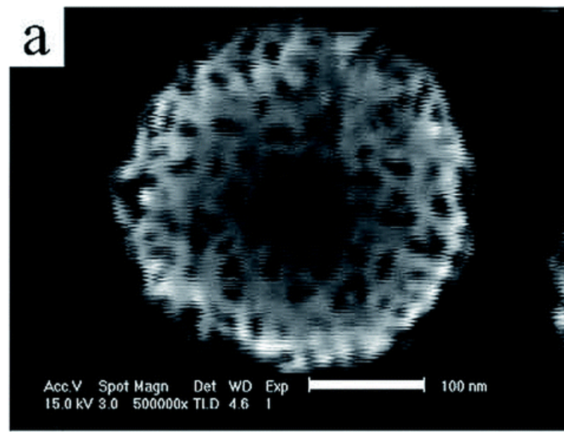

Fig.12 SEM image of nanoparticles with a porous structure after dealloying.

Regarding the catalytic activity, the literature reports on studies of PtCu film, which after the treatment of dealloying have a core-shell. The Pt-rich shell exhibits compressive strain. This change in structure has positive effects as enhanced activity for the Oxygen Reduction Reaction (ORR), a key point for the application of fuel cells and metal-air batteries [6-7].

As shown in the Fig.13 the core-shell structure is present in the PtCu alloy after the treatment of dealloying.

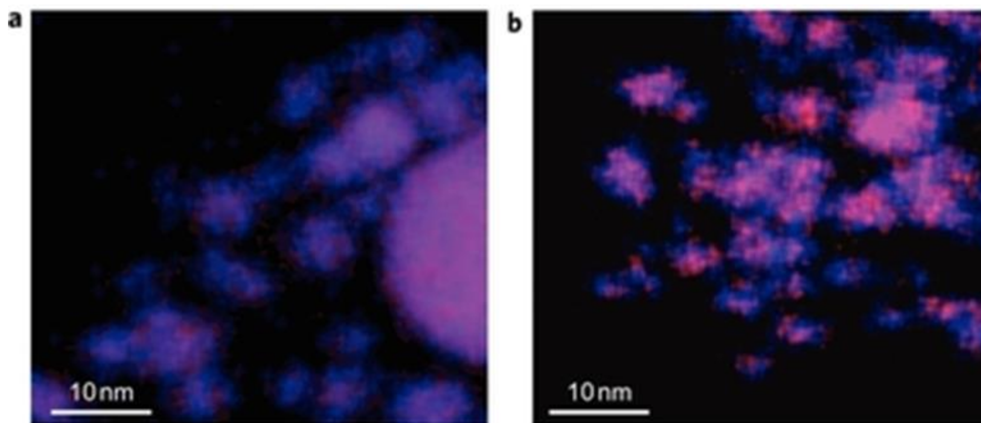

Fig.13 Elemental maps of Pt–Cu bimetallic nanoparticle: a) precursors b) dealloyed active catalysts.

Platinum has a very high melting point (1772.0 °C) and hence, a very low surface diffusivity at room temperature of order $10^{-23}cm^2/s$ as compared for example to the model Au system which has a melting point of (1064.5 °C) and a surface diffusivity of

order $10^{-16}cm^2/s$. The Cu-Pt system is one of high strain; the lattice mismatch is 8% compared to that of the Ag-Au system, which is 0.2%. These properties make the Cu-Pt system very attractive as a comparison to the Ag-Au system. The Pt-Cu system is known to especially favor small pores [8]. Considering the above graphic Fig.14, the Pt-Cu system exists as a single-phase solid solution for all compositions at elevated temperatures, and the dissolution of Cu is easily driven in acid condition where Pt is highly stable.

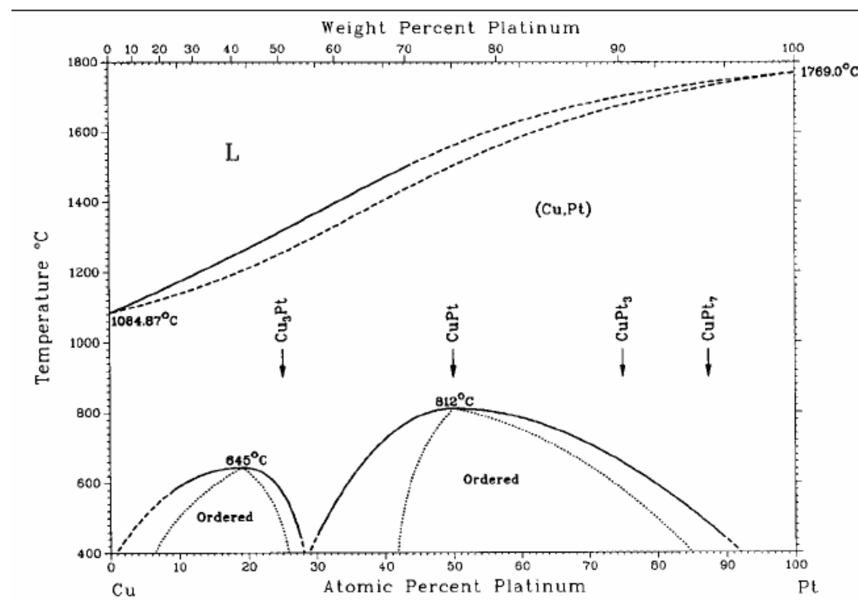

Fig.14 PtCu solid-liquid plot.

To obtain uniform platinum structure, the composition and the structure of the Pt-based alloy precursor must satisfy several requirements. First, to trigger the dissolution process, the content of the less noble metal within the alloy must be higher than the parting limit. The parting limit can be defined as the dealloying threshold for the dissolution of the less noble component from a homogeneous binary alloy. The parting limit varies from an alloy to another; in addition to its composition, the alloy must exhibit a homogeneous single phase, since the presence of any possible phase separation can alter dealloying process and thus impact the final structure of the nanoporous Pt. The parting limit for fcc structures was calculated to be 50 and 60 at% of the less noble-noble metal, under consideration of the high-density-percolation theory proposed by Artymowicz, which was experimentally proven for the Au-Ag system [6]. Although in

dealloying studies typically compositions above the parting limit are studied, in terms of catalysis the region below this threshold is more interesting. In this region the catalysts can be expected to be significantly more stable, while there is no gain in specific activity for higher compositions [7].

Fig.15 shows the typical situation of PtCu alloy after treatment of dealloying.

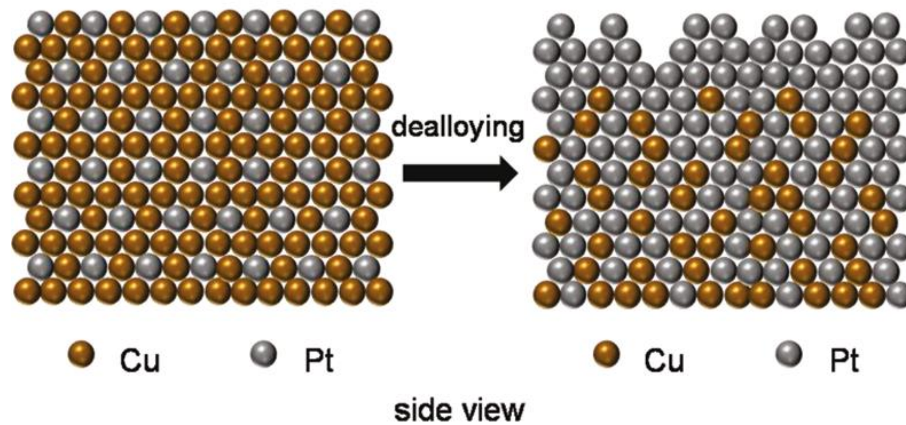

Fig.15 Situation of the coatings after the dealloying.

1.6- Substrate

The choice of the substrate on which to perform the deposition of the thin film is mainly related to limit the conditions in which the substrate itself denatures its characteristics. A high power, for example, can lead to an overheating of the substrate, or if the temperature is higher than its melting temperature, the substrate, especially if made of plastic material, can melt contaminated the deposition environment.

It must be also considered that the nature of the substrate also influence the characteristics of the film; a very important aspect concerns the cleaning and the possible treatment that is reserved to the surface of the substrate, so as to prevent foreign materials from being introduced that may interfere with the deposition process. The same contact with the hands of the operator can introduce contamination on the surface. Cleaning methods vary depending on the substrate used, as some substances can also lead to a damage of its surface: a typical example is acetone which has good degreasing ability on metals, while it has a corrosive effect on plastics.

The monolith structure of a catalyst has numerous advantages over conventional particle catalysts. These include: high specific surface, small pressure drop, good thermal and mechanical properties, simple scale up and other advantages which make them superior related to conventional catalysts [9].

The catalytic material under study was designed thinking of a practical application for heating. For this reason, a commercial SiC monolith foam [VUKOPOR®S100 from LANIK with 100 porous per inch (ppi)] was selected as support. The coatings were deposited by magnetron sputtering.

1.7- Aim of the thesis

This thesis work was carried out at Materials Science Institute of Seville, ICMS (Spain). CSIC-Univ.Seville, at the group of nanotechnology, under the supervision of the Prof. Maria Asunción Fernández.

Nanomaterials can introduce new functionalities and improved properties, while adding value to existing products and processes, in a sustainable approach. Research can start from the material itself (e.g. biomaterials), from the industrial sector (e.g. metallurgy) or from their applications (e.g. energy, health, transport). In the chemistry sector, nanomaterials are used as catalyst for various industrial processes.

In this experimental work our goal was to modify the reactivity of supported nanocatalysts, to make them attractive on an industrial scale.

Supported nanocatalysts have been produced with flexible PVD technique of magnetron sputtering. This production technique of nanocatalysts is easily applicable at industrial level. The coatings are then characterized using various spectroscopic techniques (SEM-EDX-XRD).

The Catalytic Combustion reaction of Hydrogen has considerable future potential for various applications at the industrial level, therefore, this reaction was tested for the products coatings as well as deposited and after they have undergone the treatment of dealloying. After testing the samples, the reported results were used to calculate the activation energy of the reaction CHC and the temperature of fifty percent of conversion, it is named $T_{50.}$

2- CHARACTERIZATION METHODS

2.1 Scanning electron microscope (SEM)

Scanning electron microscopy (SEM) is a microscopic technique using a beam of primary electrons, which interact with the surface of the sample, and produces secondary electrons, back-scattered electrons, characteristic X-rays, light and transmitted electrons. Signal of secondary electrons allows information on the topography and morphology of samples to be obtained, while X-rays give access to the chemical composition of the sample and elemental mapping.

SEM consists of electrons accelerated to the sample via an acceleration voltage of 2÷30 kV. The electron beam travels through electromagnetic fields and lenses, which focus the beam down toward the sample. Most incident electrons interact with specimen atoms and are scattered following different twisting paths through the sample material.

The scattering events are either elastic or inelastic. In elastic scattering, electron trajectory changes but its kinetic energy and velocity remain essentially constant, which is due to the large difference between the mass of electron and atomic nuclei. In inelastic scattering, the trajectory may be slightly disrupted, but energy is lost through interaction with the orbital electrons of the atoms on the specimen. Inelastic interaction produce a number of effects: secondary electrons, backscattered electrons, cathodoluminescence, characteristic X-rays, specimen current and transmitted electrons as illustrated in Fig.16.

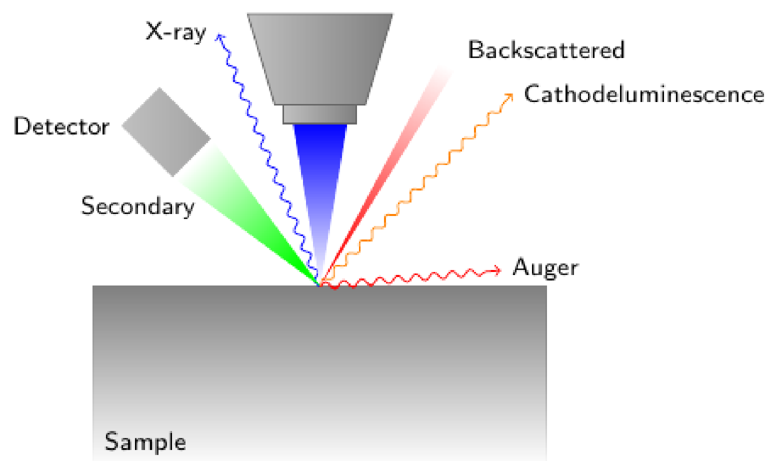

Fig.16 Mechanism of scanning electron microscopy.

The main constituent parts of a scanning electron microscope are shown in Fig.17.

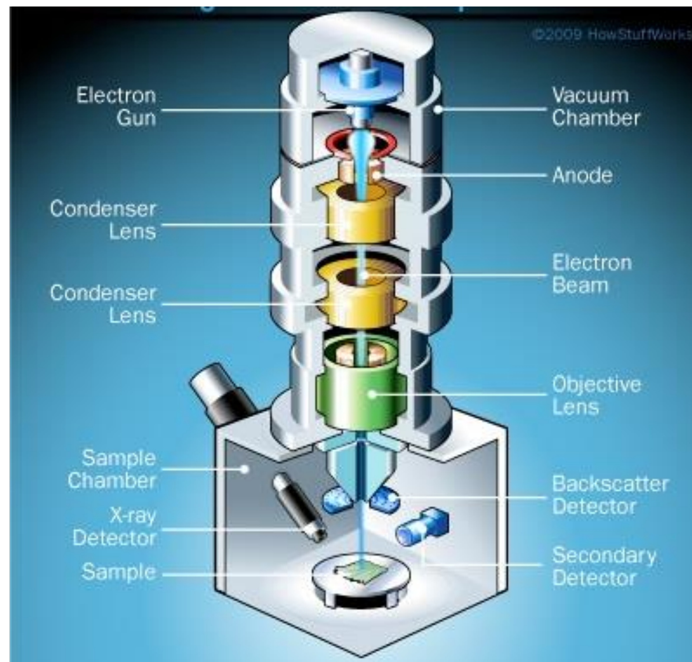

Fig.17 How SEM work.

- Beam Source: can be of two different categories: a thermionic emission or field emission. The high thermionic emission sources can in turn consist of a cathode of tungsten filament; the filament is heated to temperatures such that the electrons gain sufficient energy and eject them from the material. The electrons are then accelerated and attracted towards an anode by applying a high voltage (of the order of a few kilovolts).
- Electromagnetic lenses: are formed by a soft iron cylindrical core containing a winding, always in iron; in the winding is made to pass a current, thereby generating an electromagnetic field parallel to the axis of the lens. The court, acting on the electric charge of the electron beam, deviates its motion and reduces the diameter. Generally the instrument are installed three lenses of this type: the two said condensing lens and said objective lens. The field emission instead requires even more thrusts vacuum conditions; in it a tungsten single crystal is subjected to the action of an intense electric field applied via a first anode which causes the emission of electrons, which are accelerated toward a second anode.
- Deflection coils: their purpose is to allow the scanning line by line, in sequence, of the electron beam along a given area of the sample. They are arranged in a pair which deflects the beam along a predetermined axis and another couple that

deflects along another axis. All the system is synchronized with a cathode ray tube that goes to provide the final image.

- Signal detection system: comprises several detectors, each of which gathers information from a specific type of emission from the sample. The signal output by the detectors depends on the number of particles emitted locally and varies in brightness in the different points of the final image.

The particles emitted from the sample, because of its interaction with the electron beam consist in:

- secondary electrons: their output is used for topographical and morphological investigations on the surface analyzed and results in images with a good depth of field, high resolution and good contrast.
- Electrons diffuse back: come from the inner layers of the material, because they have a higher energy, and to assess the composition of the sample and its crystallographic characteristics, also providing images with a lower resolution.
- X-ray: the detectors dedicated to their "reading" make it possible to trace the chemical and physical composition of the test material.
- The X-ray analysis enables a compositional analysis on specimens, to be performed and can be obtained from Energy Dispersive (EDX) detection system. EDX spectroscopy is described in more detail in section 3.3.

Samples topography and morphology, as well as their chemical compositions, were studied in a high resolution microscope.

2.2-Energy Dispersive X-rays spectroscopy (EDX)

The Energy Dispersive X-ray (EDX) spectroscopy is an analytical technique used for the elemental analysis or chemical characterization of a sample. It is the analysis of the X-ray emitted by the matter in response to being hit with charged particles. At rest, an atom within the sample contains ground state (or unexcited) electrons in discrete energy levels or electron shells bound to the nucleus. The incident beam may excite an electron in an inner shell. This electron is ejected and produces an electron hole. An electron from an outer shell (on a higher energy shell) fills the hole; and the energy difference between the

two shells is released in the form of X-ray. The number and energy of the X-rays emitted from a sample can be measured by an energy dispersive detector. As the X-rays energy is characteristic of the difference between the two shells, and so of the atomic structure of the element from which the X-rays are emitted, this technique allows the elemental composition of the sample to be done. EDX spectrometer coupled with TEM is able to detect atoms with atomic number higher than 6 (Boron, Z=6); with the EDX spectrometer coupled with the SEM atoms with an atomic number equal or up to 6 are detected. Quantitative chemical composition of samples has been carried out by EDX spectroscopy. This type of analysis is possible because is present an internal standard within the instrument. The quantitative analysis changes as the electron beam energy is changed, since the scattering depth and lateral range change and change differently in different materials. The most accurate quantitative analysis is obtained when using standard materials similar to the material to be analyzed.

2.3- X-ray diffraction (XRD)

The X-ray diffraction (XRD) is a non-destructive technique that is used to study and measure the effects of the interaction between a beam of X-rays and a specific material, with the aim of analyzing the crystalline structure. In the case of thin films of this investigation method is suitable for:

•evaluation of internal stress;

•estimate of crystallographic dimensions;

•analysis of the crystalline texture;

The phenomenon of diffraction is an intrinsic characteristic of each wave and can be defined as the modification of the same wave behavior caused by the interaction with a body.

Consider a single atom: If an X-ray beam hits its electrons fluctuate around their position; when an electron slows down, it loses energy, in turn emits X-rays. In an atom the electrons are arranged in different orbits, characterized by a certain level of energy; if an atom is subjected to the electron excitation can perform an orbit jump, after which occurs the emission of X-rays. The process is shown in Fig.18.

The wavelength of the emitted radiation is indicated with $K\alpha$ and is different from material to material.

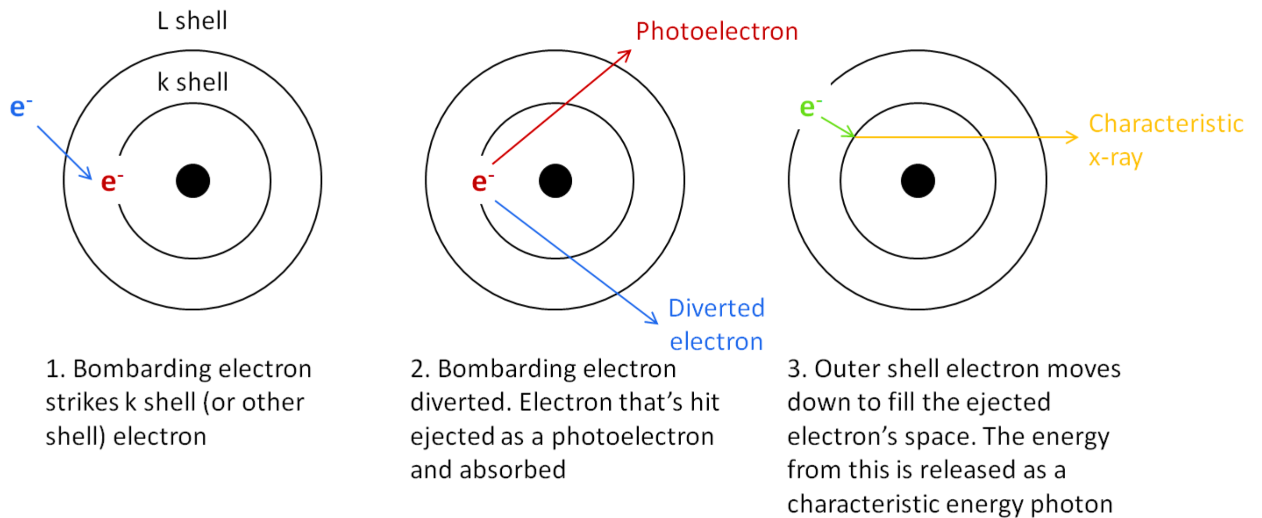

Fig.18 X-ray production.

Overall, the process of absorption and reflection of electromagnetic waves is called scattering; if in this phenomenon there is no energy difference between incident wave and reflected wave, then one speaks of elastic scattering, otherwise, if there is a loss of energy, scattering inelastic. If we assume that you have two waves that hit an atom, will be had that they can be diverted, in the same direction, by two different electrons of the same atom. they are in phase, determined with respect to the wave front, if they have traveled the same distance as a whole, before and after scattering, or if the difference between the distances covered by the two waves is an integer multiple of the wavelength of the radiation. Extending this concept to a series of atoms can be said that the diffraction is based precisely on the maintenance phase between the waves deflected by the atoms belonging to adjacent lattice planes (coherent elastic scattering), which allows to have a so-called constructive sum between them, that being in phase do not tend to cancel each other.

The phenomenon of diffraction was studied by the English physicist W. H. Bragg and his son at the beginning of '900, the two scientists explained the reason why the crystal planes reflected the rays according to certain angles of incidence. The phenomenon is shown in Fig.19. For this they developed a model that is based on the approximation of the diffraction phenomenon as a normal reflection, provided that two conditions are respected: the distance between adjacent lattice planes must be

comparable with the wavelength of the incident radiation (in fact is made of the X-rays because their wavelength is next to the typical distances present in the crystal lattices of many materials). Given the wave nature and characteristics of the crystal lattice struck by it, the reflection is not always possible, but is limited to certain angular relationships between the direction of incidence and the crystalline planes.

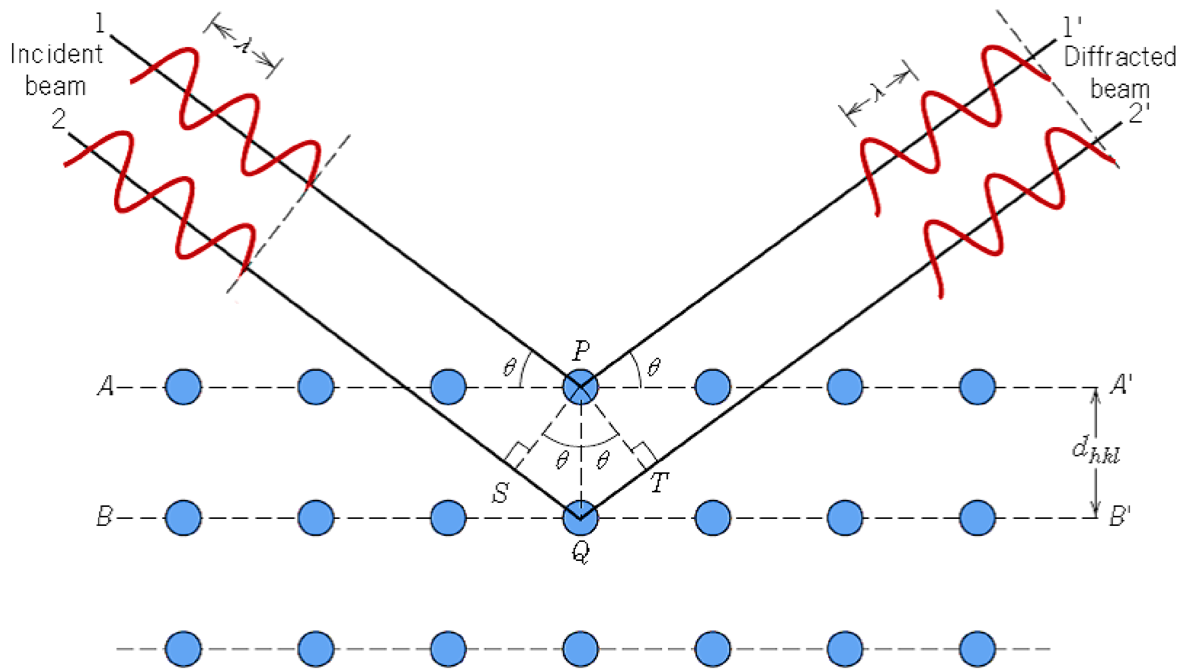

Fig.19 Model of Bragg for the X-ray diffraction.

Look at the picture above: the rays of the incident beam are always in phase with each other until the upper beam does not meet the first layer of atoms, being diverted from the atom P; the lower beam continues its path past the first layer and then be diverted from the atom Q, which belongs to the crystalline floor below.

The condition that must occur for there to be a constructive sum between the diffracted rays is that the extra SQ + QT distance traveled by the lower radius with respect to the upper one is an integer multiple of the wavelength of the two beams (λ):

$$SQ+QT=n\lambda \quad (1)$$

The distance between adjacent lattice planes d corresponds to the hypotenuse of the triangles ABz and BCz and then we have:

$$SQ=QT=d\sin\theta \quad (2)$$

where θ is the angle of incidence between the rays and the crystal planes. Since SQ = QT, from all that is derived Bragg's law:

$$n\lambda=2d\sin\theta \quad (3)$$

wherein n is an integer. The X-ray diffraction allows to obtain a diffraction spectrum, which shows the intensity of the peaks relating at certain diffraction angles. Each floor crystallographic present in the internal structure of the material in fact gives rise to the diffraction only for a given angle of incidence. For traced back to internal structure of the sample is necessary to derive the electron density, which is obtained by computing the Fourier transform of the structure factors, whose values depend on the Miller indices and the crystal structure of the material analyzed. The structure factors have a module which is equal to the square root of the intensities of the diffracted beams.

Observing the peaks can also have an idea of the amorphous component of the crystalline structure, which tends to widen the peaks themselves. A perfectly crystalline structure would entail the width of peaks almost nothing, while a highly amorphous structure it would result in a flattening of the spectrum, with no distinguishable peaks. In practice, the spectrum shows the counts of diffracted beams from the crystal for each angle of incidence considered. To all this is added often the background noise due to the disturbance caused for example by the interaction between X-rays and the air. An example of XRD spectrum for Copper is shown in Fig.20.

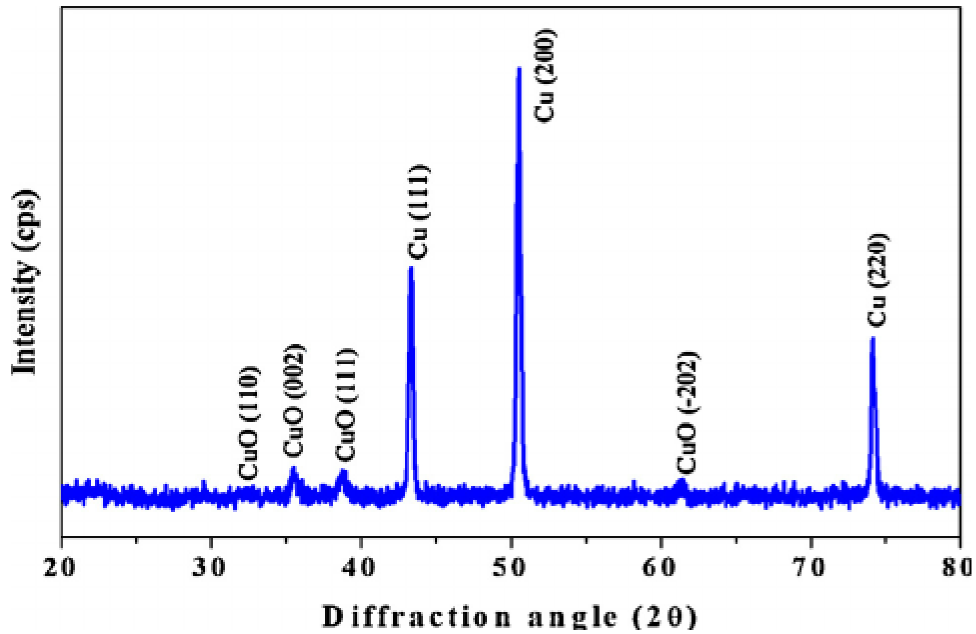

Fig.20 Diffraction spectrum for copper.

The number and position of the peaks depend on the class of the crystal and the wavelength used, while their intensity depends on the kinds of atoms and their positions in the lattice. One can also proceed to the comparison of the spectrum obtained with that of the "theoretical" material, whose structure is known, which allows to go back to the crystalline planes concerned by the phenomenon of diffraction at that particular material; this information is contained in the already mentioned database "International Tables for X-Ray Crystallography". If a peak is detected at a smaller angle than that shown in the reference spectrum is had that, for the respect of the Bragg's law, in which $n\lambda$ is a constant, the decrease of angle θ should match an increase in the distance interplanar d: therefore it means that the family of floors is subject to a tensile stress. Conversely, a greater angle of diffraction for a family of floors is to indicate a compression stress. Thanks to the analysis of the diffraction spectrum is also possible to traced back to characteristic size of the crystalline grains (or "crystallites") which constitute the internal structure of the material; This characteristic quantity can be calculated using the formula of Scherrer:

$$\text{size of the crystal grain} = \frac{K \cdot \lambda}{\cos\theta \cdot \sqrt{FWHM^2 - B^2}} \quad (4)$$

where:

K = coefficient generally equal to 0.9 (1 in the case of spherical crystals)

λ = wavelength of the incident radiation

θ = angle of diffraction

FWHM (Full Width at Half Maximum) = peak width at half height

B = instrumental error

From the formula one can guess that materials with small size of crystallites will return a spectrum consisting of several broad peaks.

RESULTS AND DISCUSSION

3 - DESCRIPTION OF THE MAGNETRON SPUTTERING SYSTEM

The practical part of this thesis activity was characterized by the realization of a thin platinum and copper film deposited on a silicon carbide substrate and the subsequent characterization from a morphological and structural point of view. Fig.21 shows globally the magnetron sputtering process.

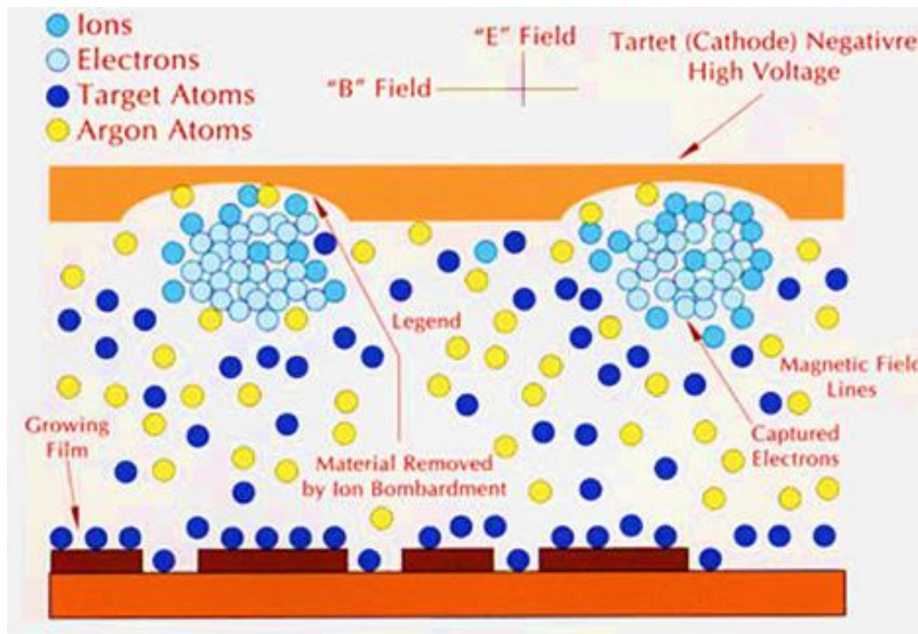

Fig.21 Magnetron sputtering process.

For the realization of thin films, a magnetron sputtering system was used. It is included in the research laboratory "Isla Cartuja" of the University of Seville; it consists of a deposition chamber, a pumping system, a cathode with permanent magnets, a cooling system, the power supply unit and a system of interlocks necessary for the safety. Fig.22 shows the chamber magnetron sputtering used for this thesis.

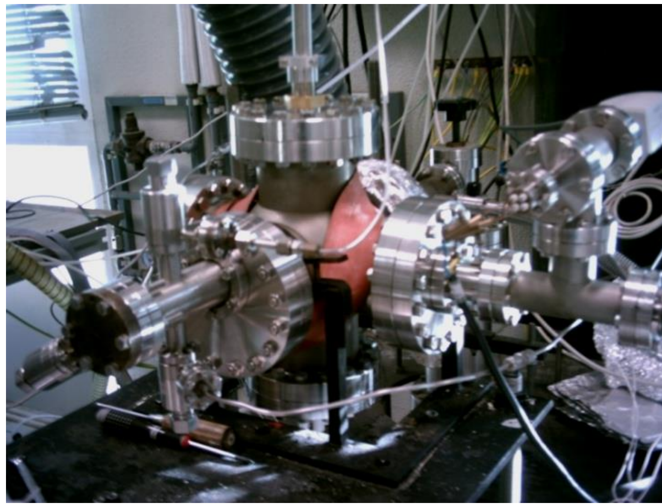

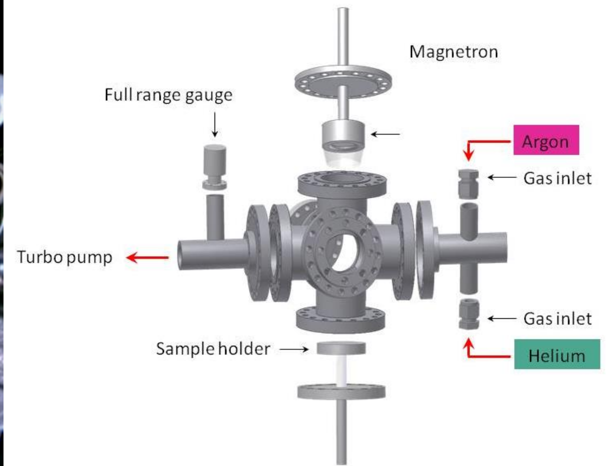

Fig.22 The magnetron sputtering system employed in this experimental thesis.

The environment in which it was made is sputtering a stainless steel container of parallelepiped shape, a side of the chamber consists of a circular door with a gasket and a small window that allows the operator to look inside the room. Inside the chamber there are two disks positioned above the cathode. The lower disk is the "shutter". Turning the shutter, through a controlled mechanism from the outside, you can cover the cathode. This system is necessary to be able to control the start of deposition conditions. The top disk instead serves to support the substrate and is supported by a rod adjustable in height, so as to change the distance between the cathodes and the substrate itself. The inner walls of the chamber are in direct contact with the plasma during the process and are then coated stainless steel panels that can be removed to enable their cleaning. The deposition chamber is equipped with four ceramic resistances used to pre-heat before deposition allowing to reduce as much as possible the water amount adsorbed on the chamber walls (baking). The baking temperature is controlled with the thermocouple. The system that allows the creation of vacuum in the deposition chamber is the combination of a rotary pump and a turbomolecular pump: the first is used to reach a preliminary vacuum condition, in that moment intervenes the second, which allows to get the best conditions vacuum. There is also a set of valves responsible for the placing of the process gas in the chamber (99.9995% pure argon), (99.9995% pure helium) and the air inlet at the end of deposition, in order to restore the room atmospheric pressure.

The cathode is placed on top of the chamber, above the shutter, it is planar and circular in shape. The cathode can accommodate a target with a diameter of two inches

and is provided with permanent magnets in their turn immersed in the cooling liquid (water). It is necessary to provide cooling of the permanent magnets and the turbomolecular pump and for this is used a closed circuit in which refrigerated water flows, controlled by a cooling system, with a variable water flow rate from 8 to 30 L/min.

It is chosen and to operate with the technique that takes the name of cosputtering, varying the composition of a copper target by two inches (99.99%, 1 mm thick), with the addition of fifteen platinum strips (99.99%, 1 mm thick), each of which it was 1mm wide. The fifteen strips were anchored on the copper target with the copper tape as shown in Fig.22.

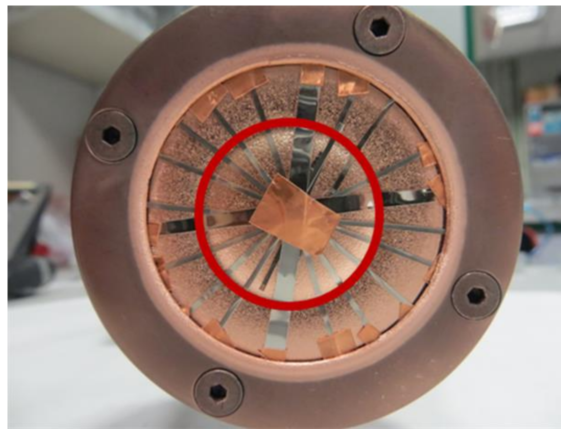

Fig.23 Magnetron sputtering target.

The result of the deposition of magnetron sputtering is shown in Fig.24 (a,b).

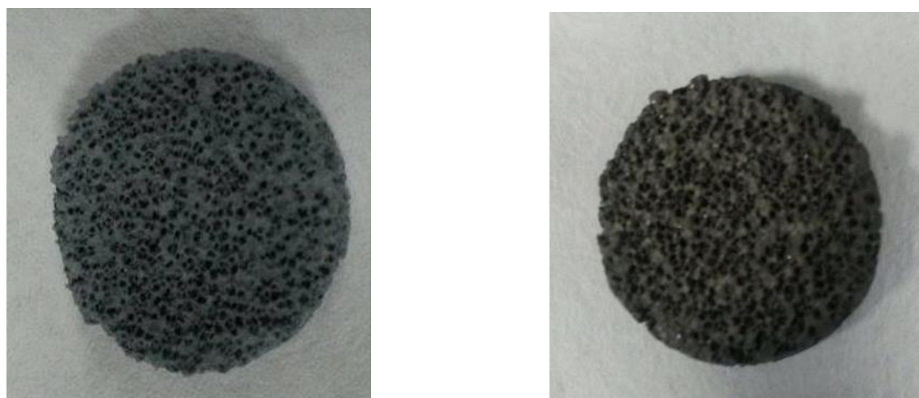

Fig.24 a) Only SiC b) PtCu on SiC.

3.1 - Characterization of the samples by XRD

The analysis on the deposited on the silicon film was performed with a range for the diffraction angle 2θ ranging from 38° to 54°. The spectra obtained were compared with that of copper and platinum standards reported in the archive ICDD (International Center of Diffraction Data). The XRD study of the PtCu catalytic material after dealloying on Si(100) in comparison with the PtCu as deposited and pure Cu. X-ray diffraction profiles of the as-deposited PtCu, Cu and dealloyed PtCu films on Si(100) are shown in Figs.(25-26).

PtCu films as deposited show single phase centered cubic (fcc) structures. The diffraction peaks of dealloyed PtCu shift toward lower 2θ and are broader compared to the as deposit PtCu, showing that Cu is leached from PtCu alloy and that the microstructure becomes more disordered with a smaller grain size. In addition, the dealloyed diffraction peaks are asymmetric, indicating the formation of a no uniform structure after the selective leaching.

Observing the values is noted that some peaks are in correspondence of slightly smaller angles of their position "theoretical reference". For example, the main peaks appears to be in advance in both cases and this indicates that the planes (111) and (200) may be subjected to the tensile internal stress. Only the peak (111) of $PtCu_3$ into helium Fig.24, shows a slight delay, which could represent a compression stress. The as-deposit PtCu thin film is uniform, well alloyed and single phase.

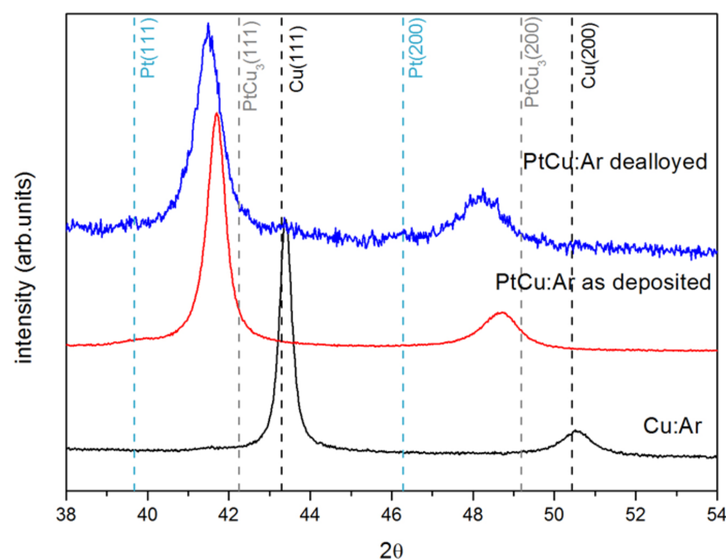

Fig.25 XRD plot for samples under Argon.

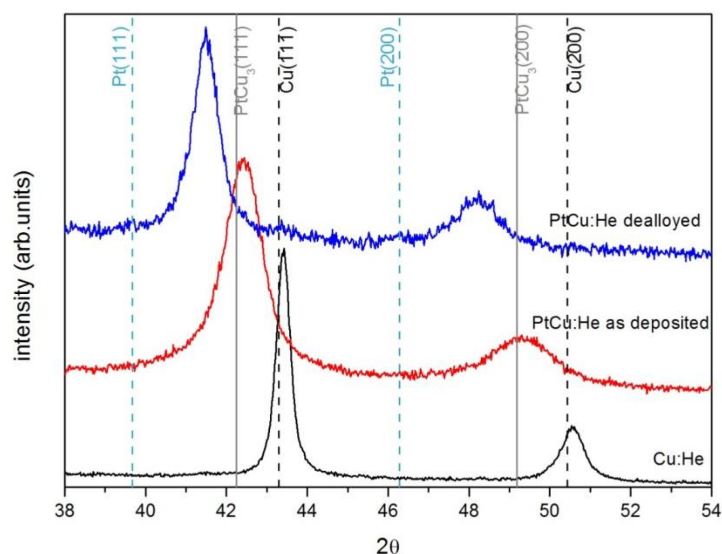

Fig.26 XRD plot for samples under Helium.

The sizes and the lattice strain of the particles of the alloys have been obtained using Sherrer's formula, with the selected peaks (111) and (200). The results are shown in Tab.1-2.

Tab.1- Lattice strain in the samples.

Lattice strain	**%**
Cu:He RF 250nm	0,4±0,1
$PtCu_3$:He RF 300nm	1,6±0,1
$PtCu_3$:He RF 300nm_dealloyed 5'	2,6(111)- 2,8(200) ±0,1
Cu:Ar RF 400nm	0,3±0,1
$PtCu_3$:Ar RF 400nm	0,6±0,1
PtCu3:Ar RF 400nm_dealloyed 5'	0,8(111)- 1,2(200) ±0,1

Tab.2- Size of the crystals in the sample.

Cristal size	**Nm**
Cu:He RF 250nm	32±1
$PtCu_3$:He RF 300nm	7±1
$PtCu_3$:He RF 300nm_dealloyed 5'	4 (111), 3 (200) ±1
Cu:Ar RF 400nm	38±1
$PtCu_3$:Ar RF 400nm	21±1
PtCu3:Ar RF 400nm_dealloyed 5'	13(111), 8 (200) ±1

3.2 Pt-Cu coatings: microstructural characterization by SEM

In this section the SEM characterization of the coatings is presented. The difference between the two coatings (thickness range 300÷400 nm), regards the deposition gas employed during the sputtering magnetron. The two gases used are helium and argon; Radiofrequency (RF) has been always chosen as type of power supply.

3.3- Pt-Cu coatings under helium: microstructural characterization by SEM

The following samples have been analyzed by high resolution SEM-FEG microscope Hitachi S4800 operating at 5 keV, at different magnifications:

- The coatings as deposited on Si and SiC Figs.(27-29);
- After the dealloying treatment carried out with 14,4 M HNO_3 Figs.(30-32);

The study of the microstructure and chemical characterization of PtCu coatings on SiC is essential to fully understand the consequent kinetic behavior of these films. As a guideline the coatings were characterized by SEM before and after the dealloying to emphasize the changes that this technique leads to the structure of the films. The following imagines show a uniform distribution of the alloy on the support.

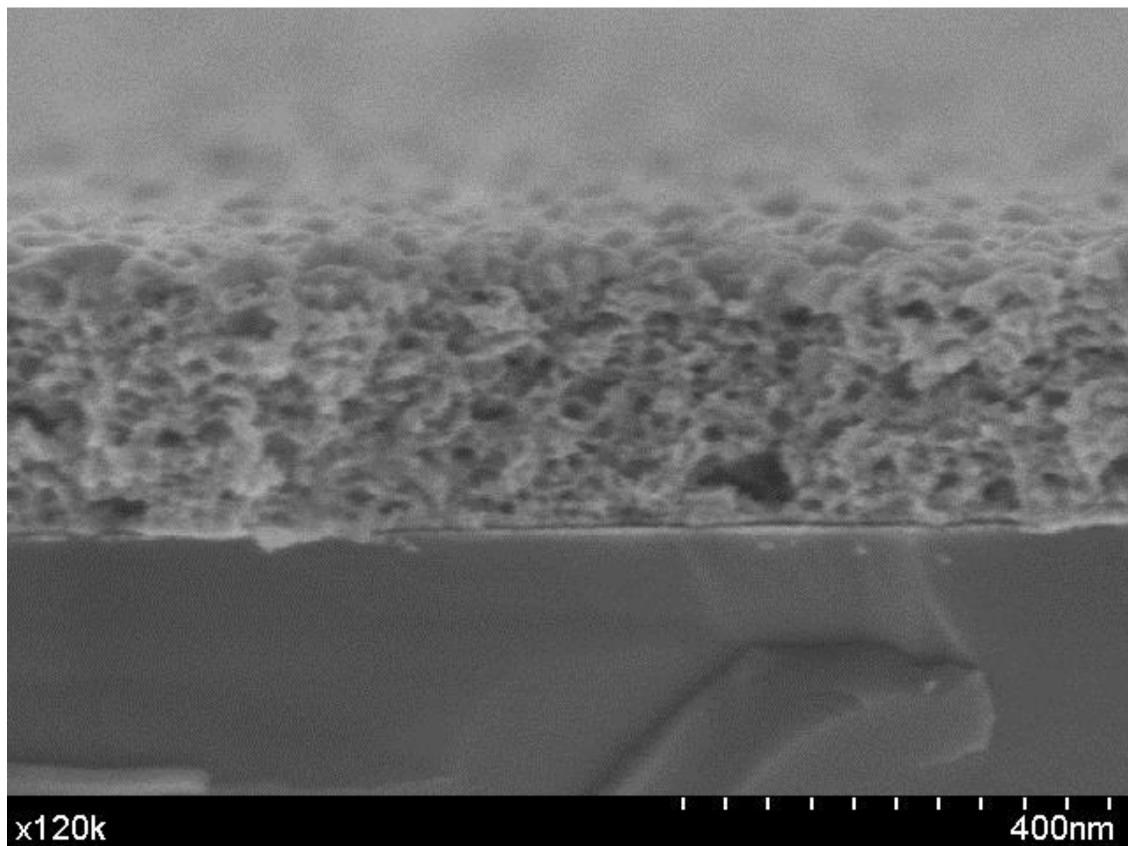

.

Fig.27 PtCu, He, 300 nm on Si cross section.

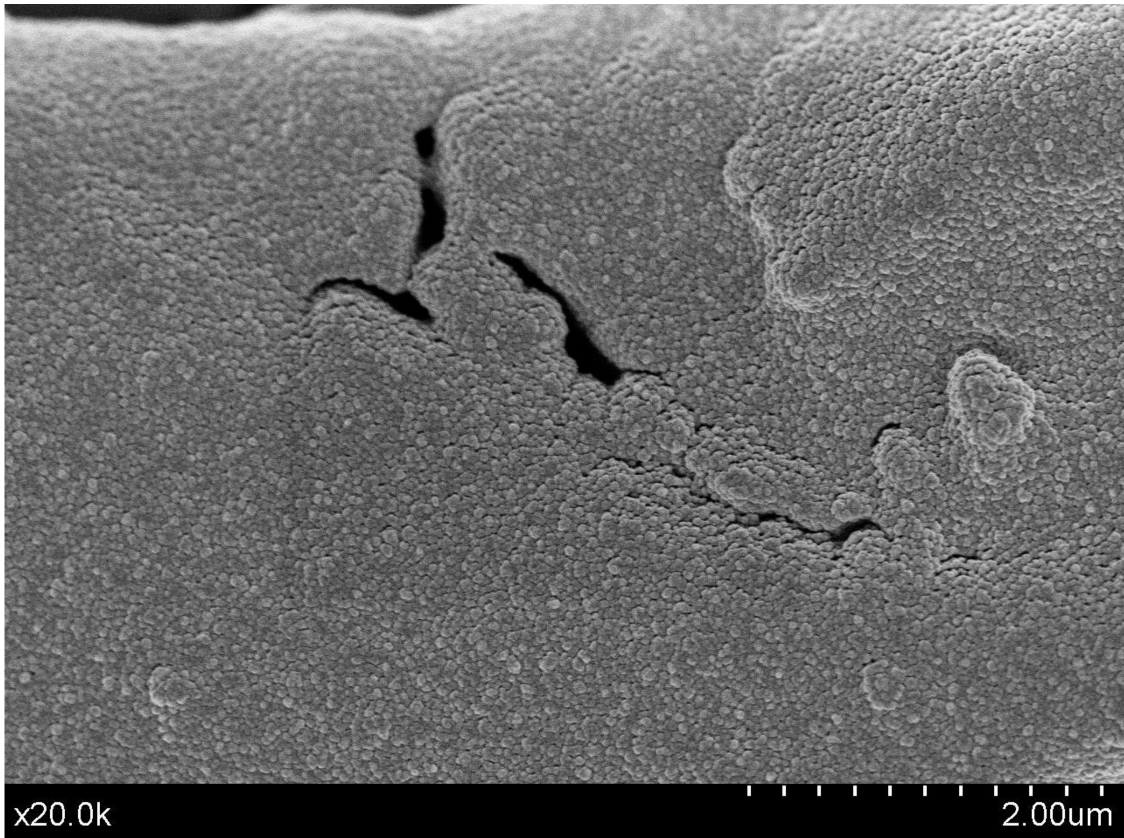

Fig.28 PtCu, He, 300 nm on SiC top view.

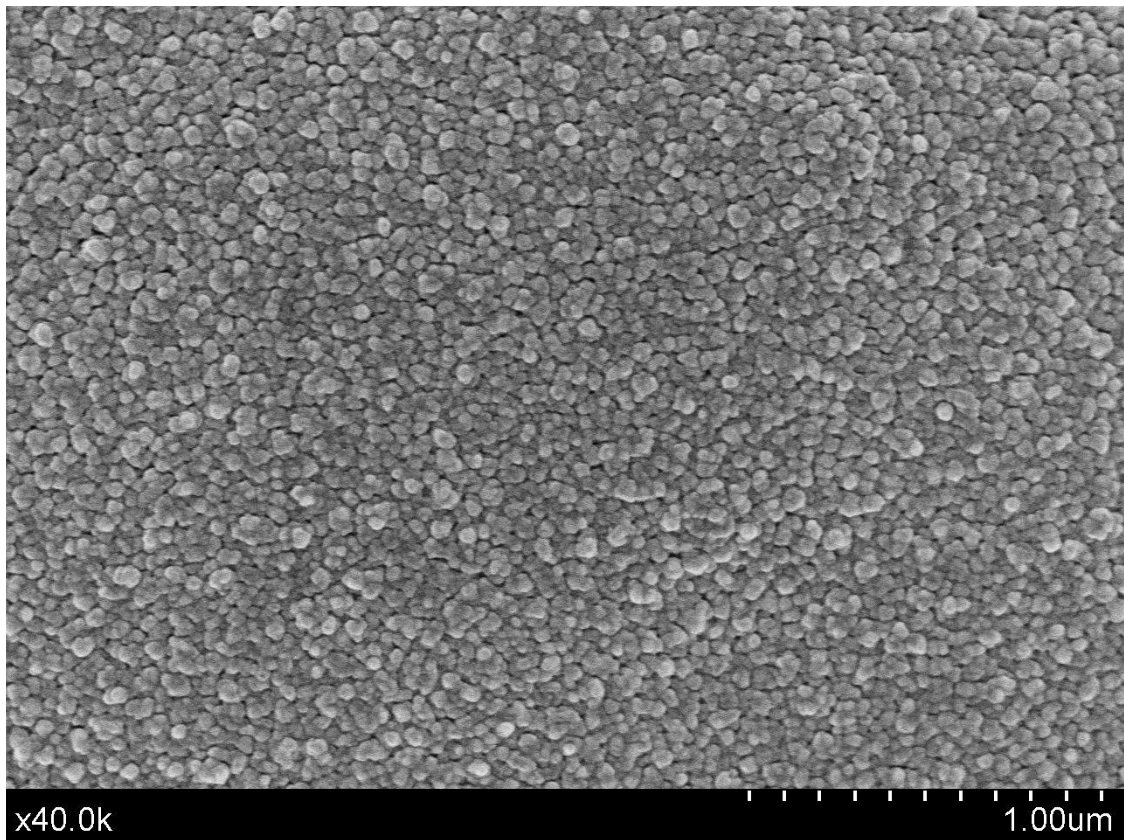

Fig.29 PtCu, He, 300 nm on SiC top view.

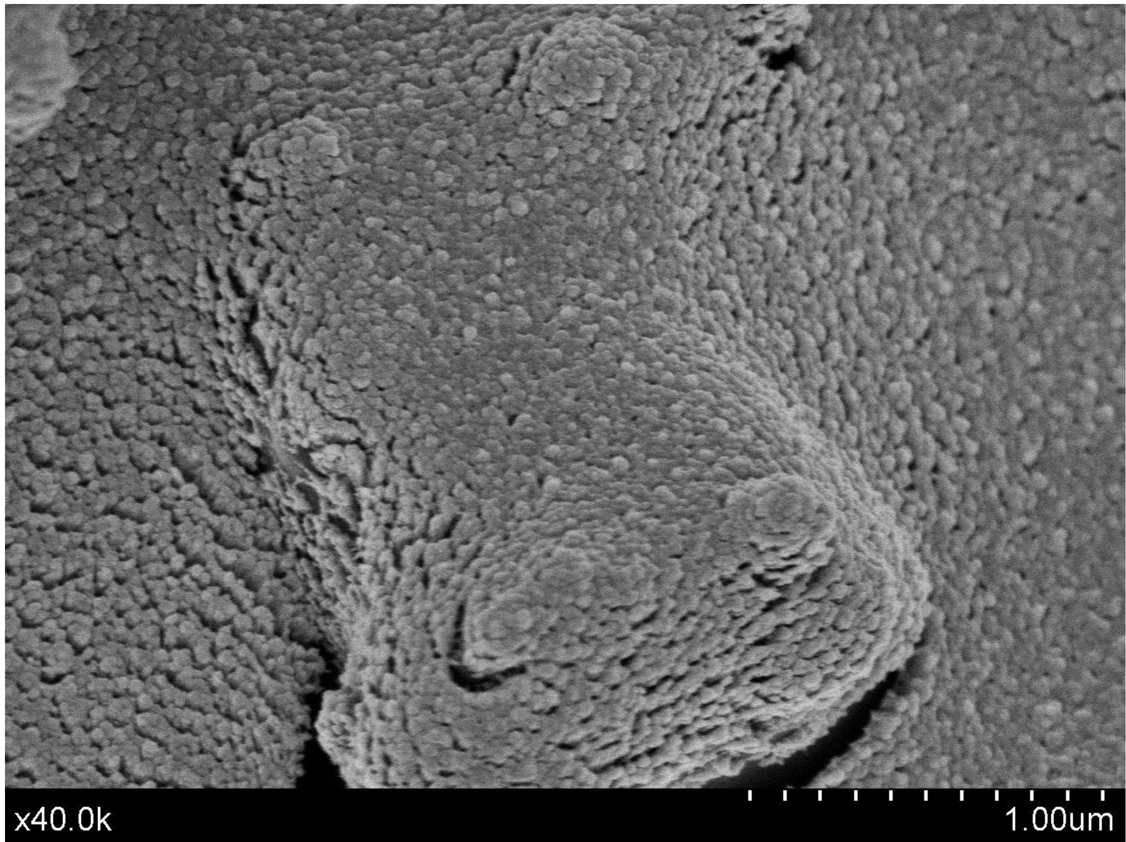

Fig.30 PtCu, He, 300 nm on SiC: SEM top view after 5’ of dealloying in a 14,4 M HNO_3 acid solution.

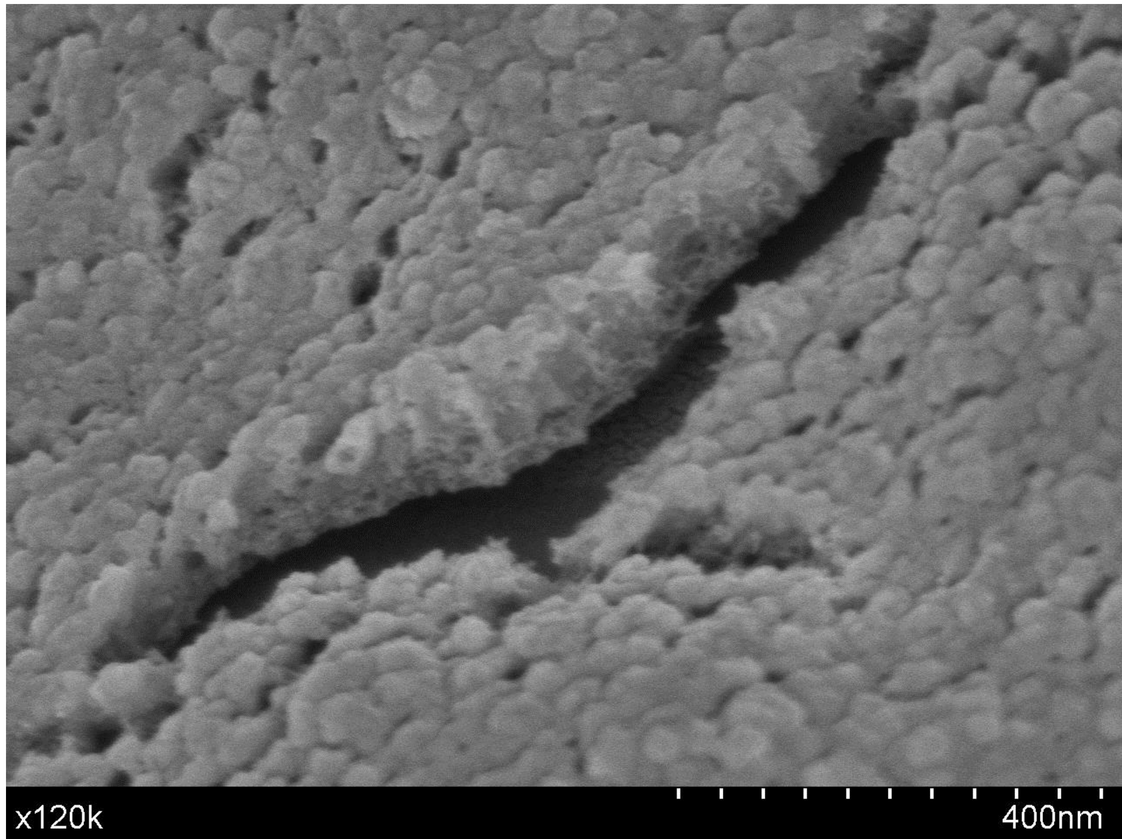

Fig.31 PtCu, He, 300 nm on SiC: SEM top view after 5’ of dealloying in a 14,4 M HNO_3 acid solution.

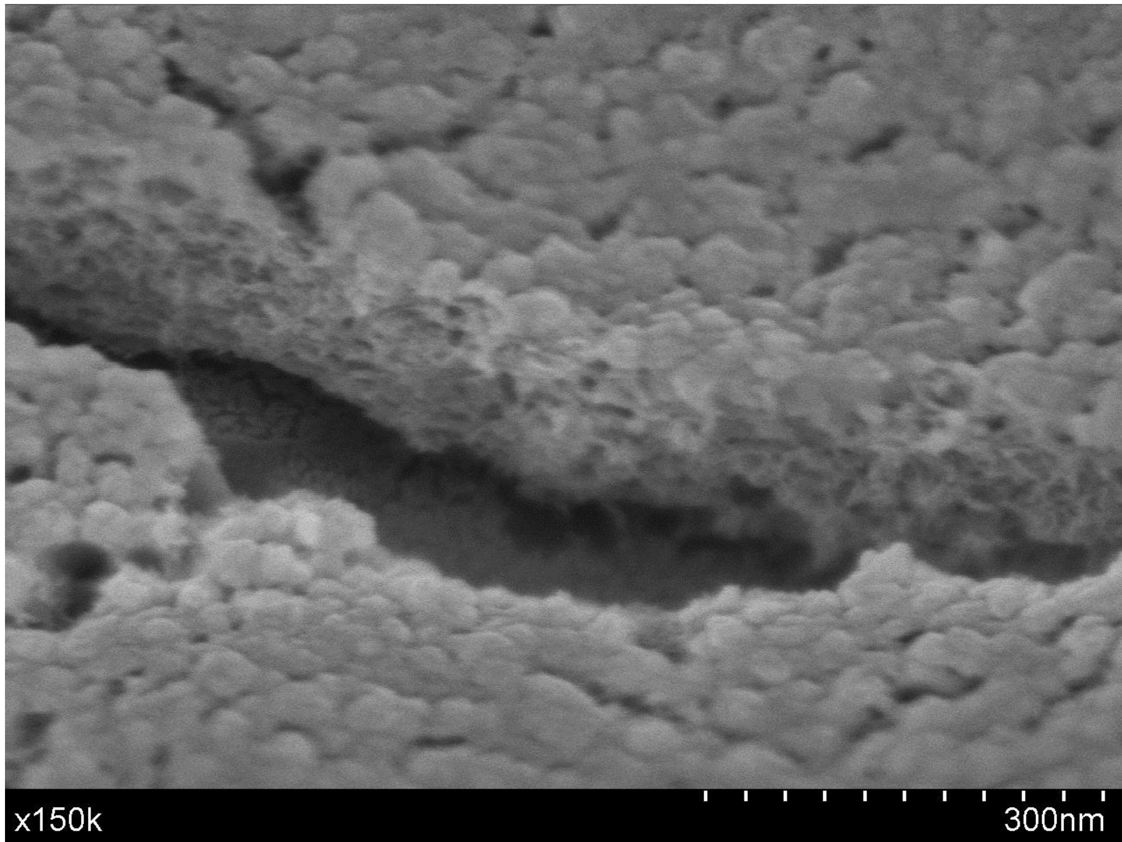

Fig.32 PtCu, He, 300 nm on SiC: SEM top view after 5' of dealloying in a 14,4 M HNO_3 acid solution.

The SEM images show that the coatings have a porous open structure that facilitates the passage of the acid during dealloying.

3.4- Pt-Cu coatings under argon: microstructural characterization by SEM

The following samples have been analyzed by high resolution SEM-FEG microscope Hitachi S4800 operating at 5keV at different magnifications:

- The coatings as deposited on Si and SiC Figs.(33-34);
- After the dealloying treatment carried out with HNO_3 14,4 M Figs.(35-37);

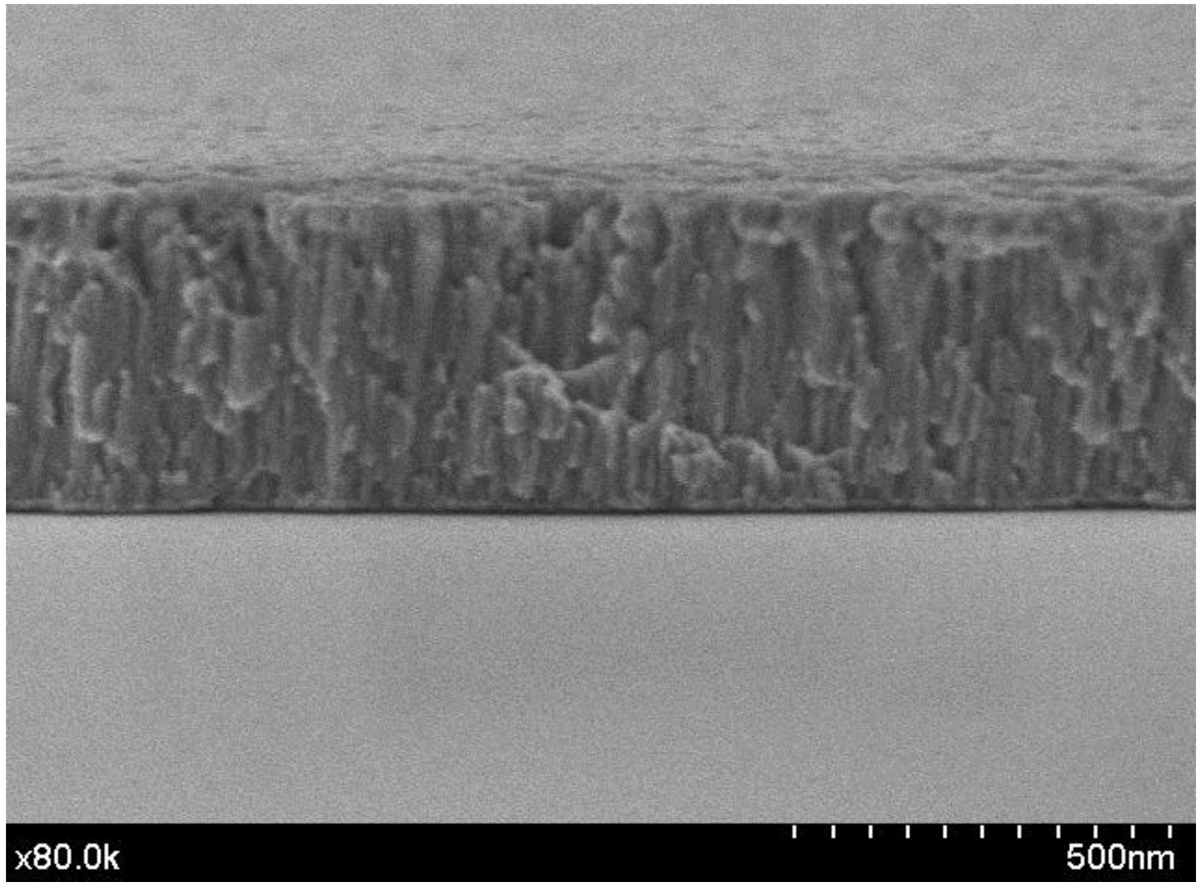

Fig.33 PtCu, Ar, 400 nm on Si cross section.

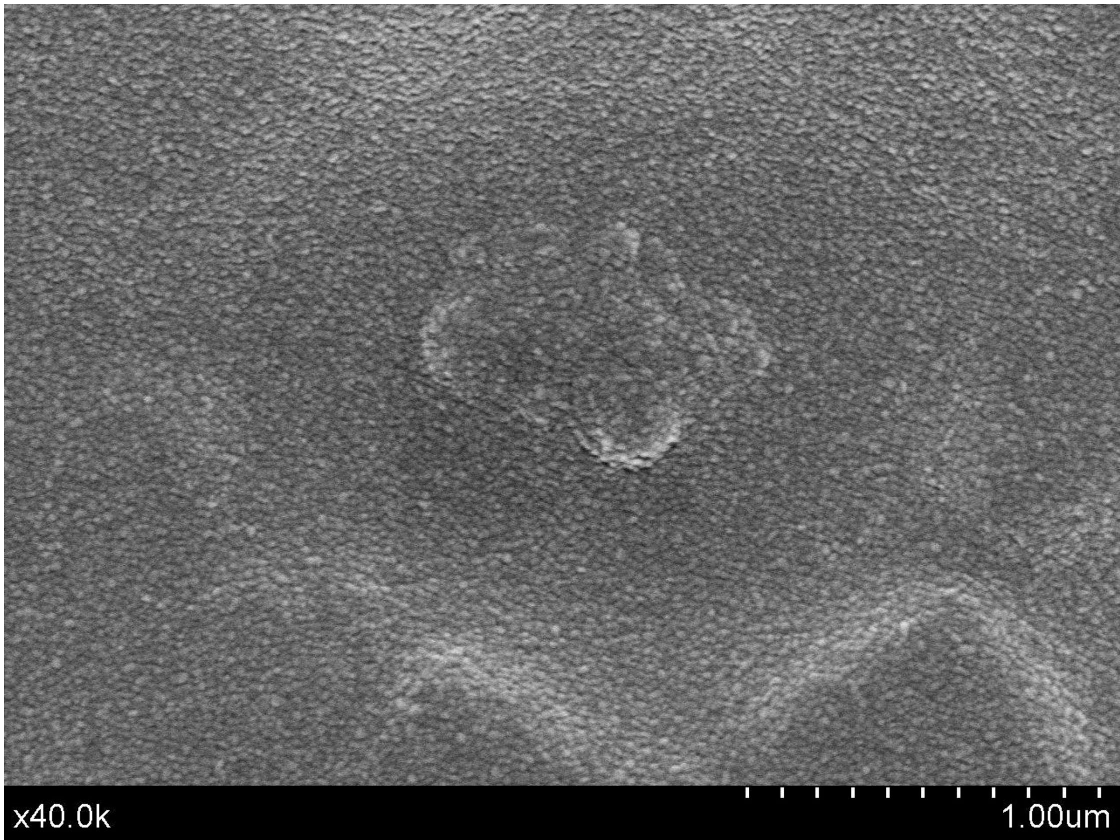

Fig.34 PtCu, Ar, 400 nm on SiC, SEM top view.

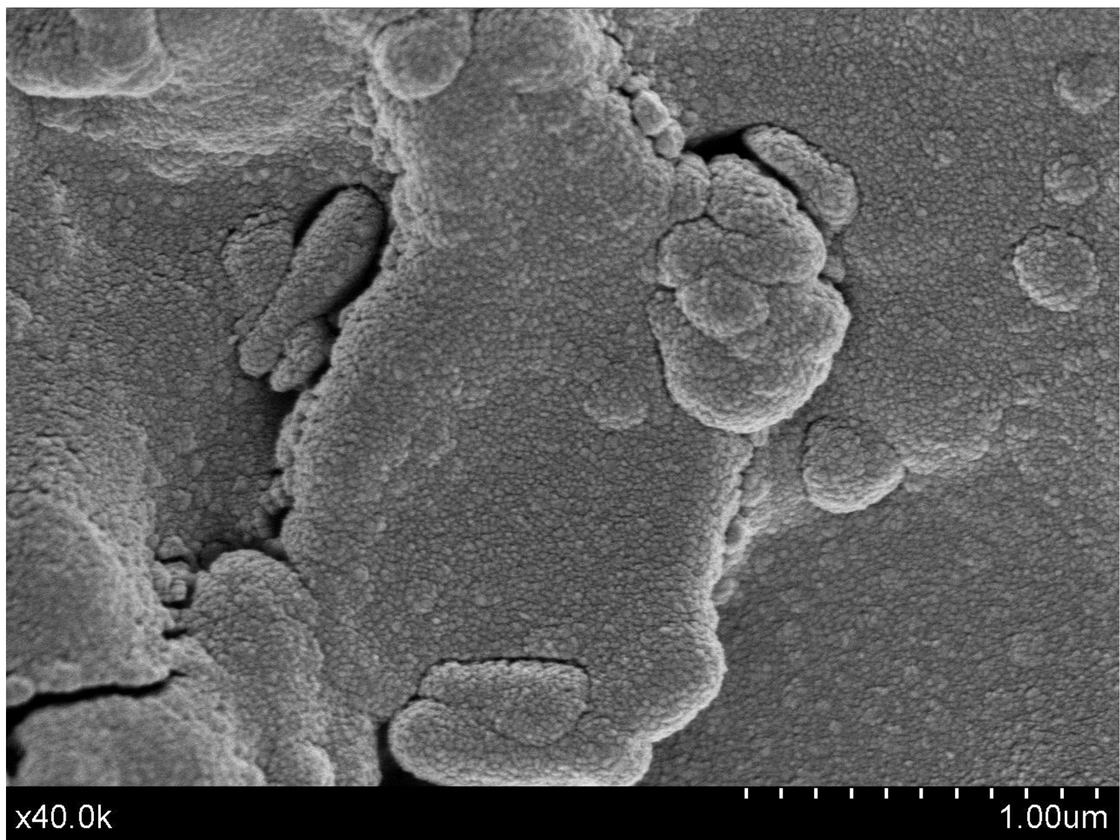

Fig.35 PtCu, Ar, 400 nm on SiC, SEM top view after 5' of dealloying in a 14,4 M HNO_3 acid solution.

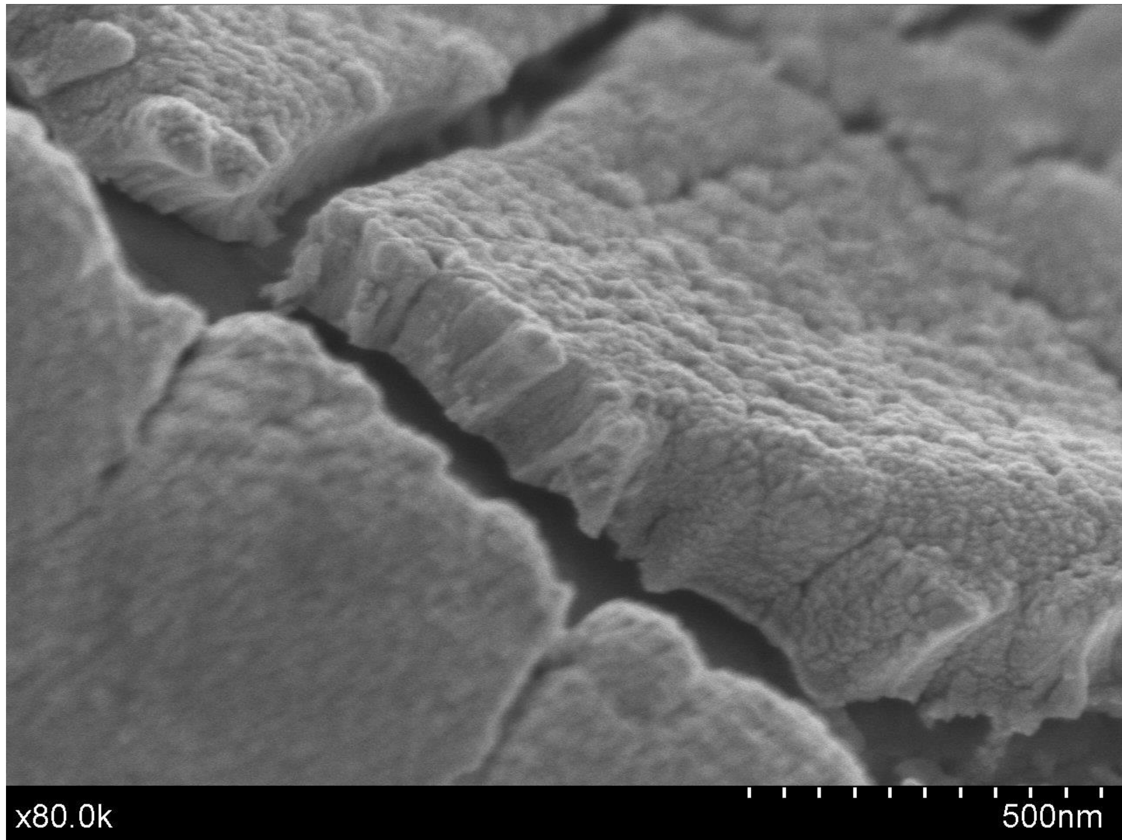

Fig.36 PtCu, Ar,400 nm on SiC, SEM top view after 5' of dealloying in a 14,4 M HNO_3 acid solution.

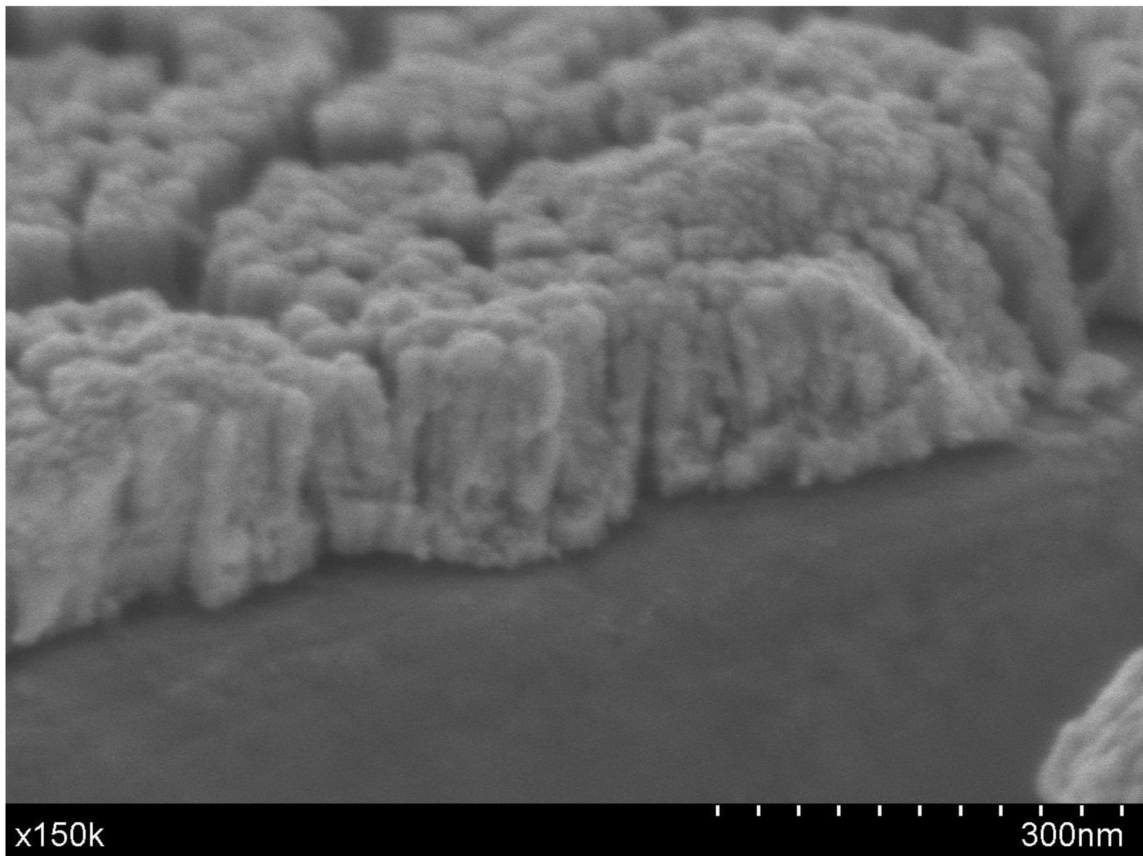

Fig.37 PtCu, Ar, 400 nm on SiC, SEM top view after 5' of dealloying in a 14,4 M HNO_3 acid solution..

Differently the speech for the coatings grown under argon, they present a more dense columnar structure, with a tighter porosity. Indeed this hypothesis is confirmed because in the same time interval manage to dissolve less copper than helium samples.

3.5- Pt-Cu coatings: Microstructural characterization by EDX

The coatings have similar thicknesses, so for a good comparison has been chosen to work with EDX 20kV spectra obtained from general areas. On coatings deposited on SiC had been carried quantitative spectroscopic analysis, to demonstrate the presence and the homogeneous distribution of platinum on the coating. The EDX spectroscopy confirms the presence of platinum Figs.(37-38). The composition of the coatings on SiC are shown in Tab.3 and were determinate by quantitative analysis giving the values of 56,00% of Cu and 44,00% of Pt under argon gas and 82,12% of Cu and 17,88% of Pt under helium gas. By the graphs in the Fig. (38-39), are noted that after the dealloying the amount of copper decreases and that of platinum increases. For the coatings under argon gas, Before dealloying has been found an initial value Pt/Cu atomic ratio of 0,79 passing to 0.99 after dealloying (atomic value); instead for coatings under helium gas Pt/Cu ratio increased from 0.22 before dealloying passing to 4,92(atomic value). From these values has been deduced that the increase of quantities of platinum is much greater for coatings under helium gas compared to those under argon gas.

Tab.3 -composition of the alloy by EDX analysis.

Sample	Cu%	Pt%	Pt/Cu	Sigma mean
PtCu_He_RF_37min	82,12	17,88	0,22	0,85
PtCu_He_RF_37min_dealloying_5min	16,89	83,11	4,92	0,46
PtCu_He_RF_37min_dealloying_10min	12,60	87,40	6,94	0,87
PtCu_Ar_RF_7,30min	56,00	44,00	0,79	1,02
PtCu_Ar_RF_7,30min_dealloying_5min	50,30	49,70	0,99	0,66
PtCu_Ar_RF_7,30min_dealloying_10min	49,02	50,98	1,04	0,98

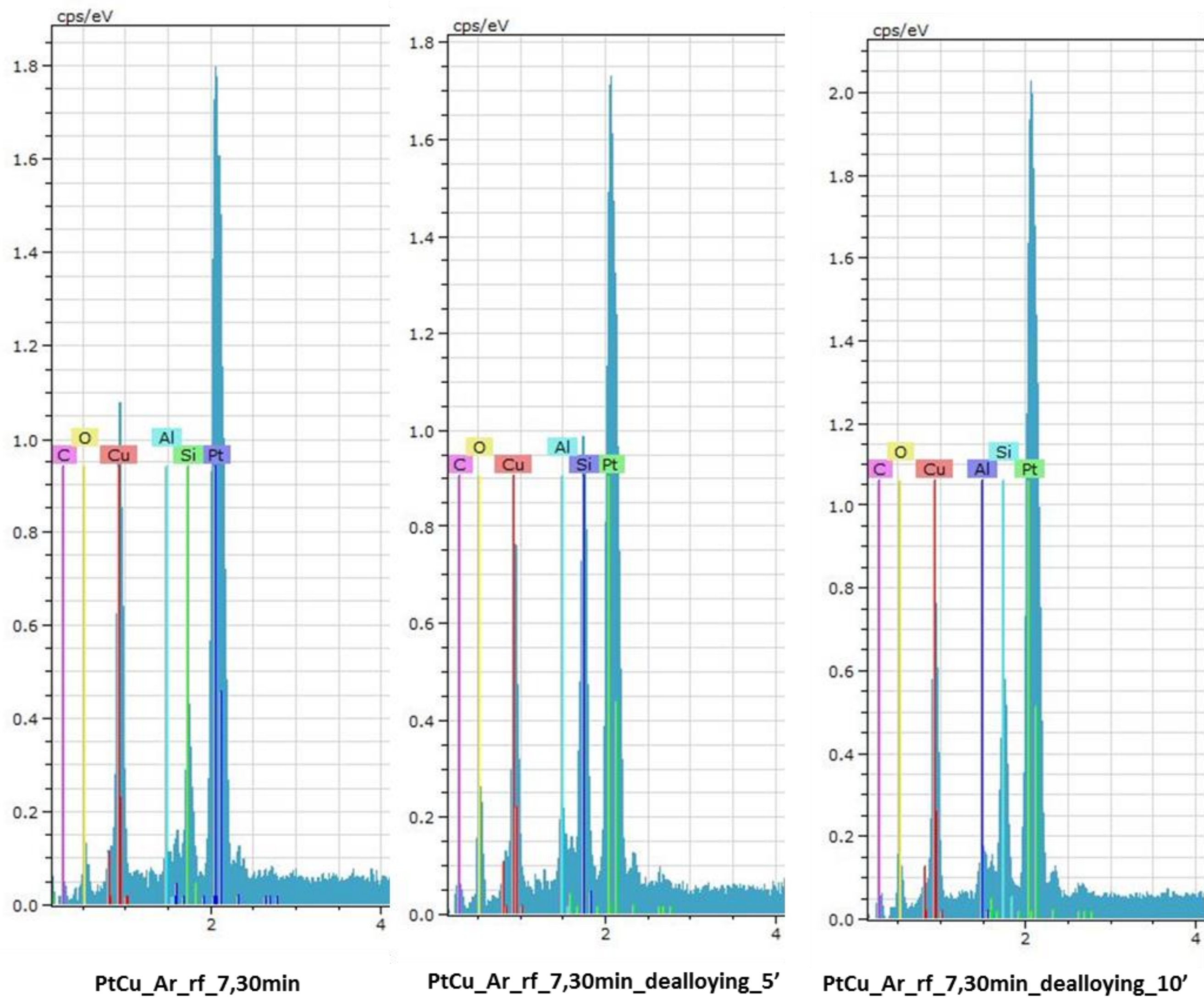

Fig.38 EDX analysis for samples under Argon.

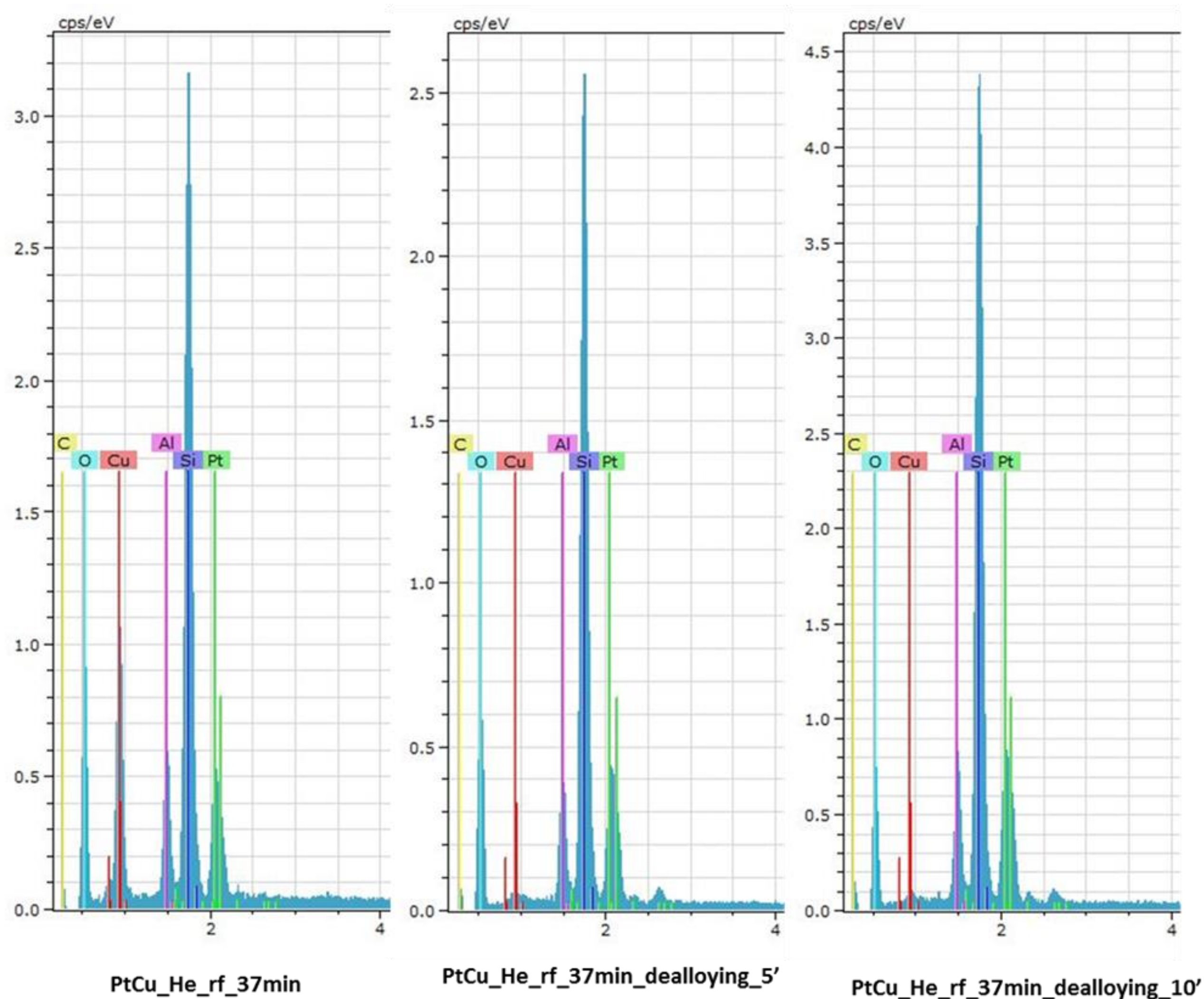

Fig.39 EDX analysis for samples under Helium.

An element map is an image showing the spatial distribution of elements in a sample. Because it is acquired from a polished section, it is a 2D section through the unknown sample. Elemental maps obtained by EDX 20kV are shown in Figs.(40-43) and permit to distinguish and quantifying the presence of majoritarian elements (Pt and Cu), and Si, C, O, Al. The microstructure of these coatings may be considered as platinum nanoparticles dispersed on a matrix of copper supported on porous SiC. It is noted that the two metals are homogeneously distributed over the support.

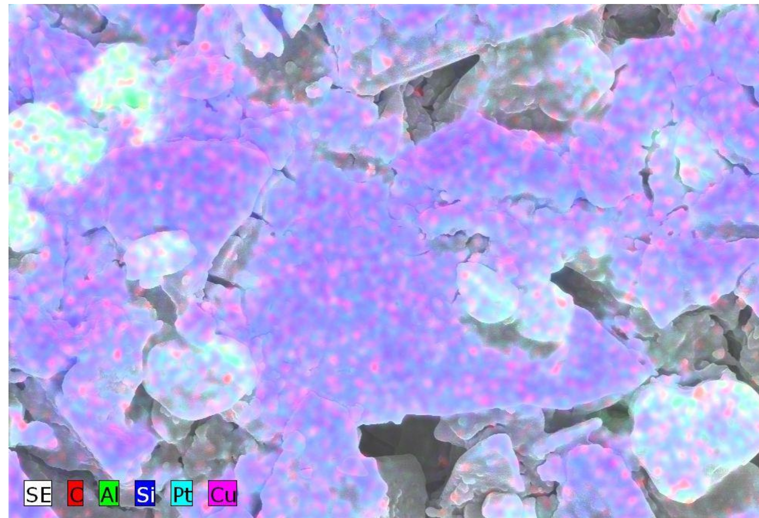

Fig.40 Global elemental mapping.

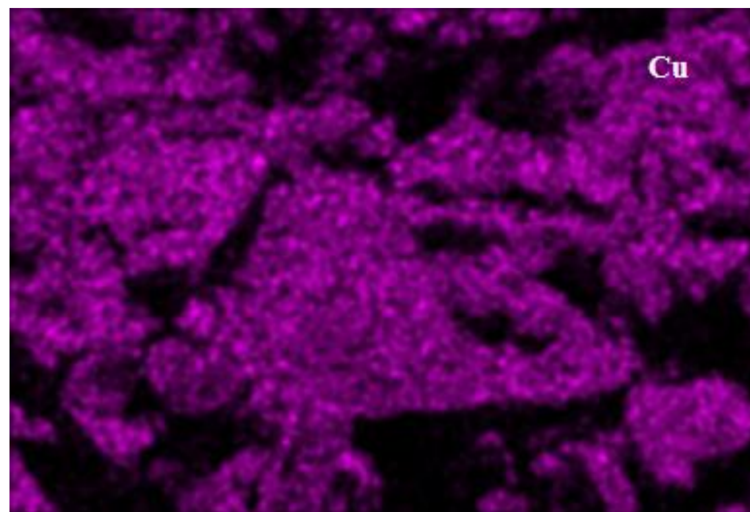

Fig.41 Elemental mapping of Cu on SiC.

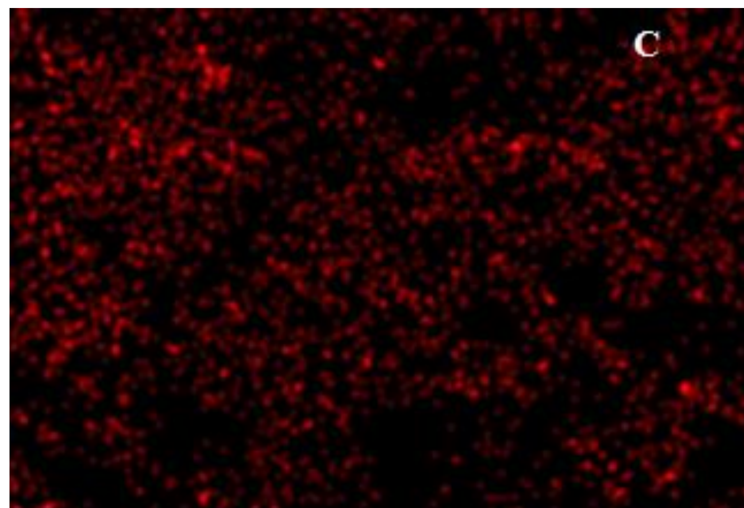

Fig.42 Elemental mapping of C on SiC.

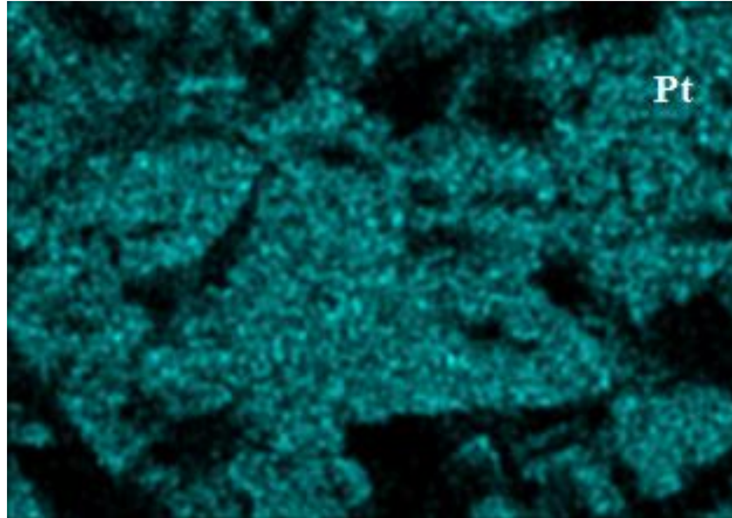

Fig.43 Elemental mapping of Pt on SiC.

3.6-Conclusion

Coatings containing platinum and copper on SiC, have been obtained with the technique of magnetron sputtering. These alloys have a thickness ranging from 300 to 400nm. Platinum and copper result homogeneously distributed, as can be seen from SEM images and Elemental mapping.

Moreover as shown by SEM images in the coatings with helium gas, the presence of porosity with an open structure can be noted, this leads to a greater increase of platinum on the surface after the dealloying, which means an increase of reactivity. The coatings grown under argon show a more closed porosity, a first effect of this change in porosity is a smaller quantity of dissolved copper during the dealloying.

Quantitative analysis using EDX spectroscopy conducted on coatings deposited on SiC, confirmed the platinum increased after the treatments of dealloying.

The experimental values of the size of the crystal grains obtained with the Sherrer formula were compared qualitatively by comparing SEM images of pure copper deposited by magnetron sputtering under argon and helium. It is clearly visible that the pure copper grains are much larger than those of the alloys.

In conclusion the technique of magnetron sputtering leads to the formation of PtCu coatings well distributed on of the SiC substrate.

3.7 - Catalytic hydrogen combustion CHC

Talking about renewable energy a current topic is pollution due to the use of fossil fuels. The use of H_2 would have the advantage of using the fossil sources to get gas directly (starting from methane, for example).

Hydrogen is advantageous because presents catalytic ignition at lower temperatures, the feasibility to adopt inexpensive oxide catalysts, and no generation of carbon-based residues [10]. The H_2 then used as fuel in transport, reacting with oxygen, produce as the only waste product water, completely eliminating CO_2 emissions and climatic and environmental problems associated with them.

The combustion reaction in the air is the following:

$$\mathbf{2H_2(g) + O_2(g) \rightarrow 2H_2O(l)} \qquad (5)$$

Reaction (5) is highly exothermic (−286 kJ mol^{-1}) and can be controlled using appropriate catalysts, in contrast to flame combustion which produces NOx and presents well-known safety issues such as flashback possibility [11, 12].

Hydrogen and oxygen in presence of a suitable catalyst may be combined at temperatures significantly lower than flame combustion (from room temperature to 500 °C). This principle can be used to design catalytic burners and heaters. Catalytic burners require considerably more surface area than conventional flame burners. Therefore, the catalyst is typically dispersed in a porous structure. The reaction rate and resulting temperature are easily controlled by controlling the hydrogen flow rate. The reaction takes place in a reaction zone of the porous catalytic sintered metal cylinders or plates in which hydrogen and oxygen are mixed by diffusion from opposite sides. A combustible mixture is formed only in the reaction zone and assisted with (platinum) catalyst to burn at low temperatures Fig.44. The only product of catalytic combustion of hydrogen is water vapor.

Due to low burning temperatures there are no nitrogen oxides formed. Possible applications of catalytic burners are in household appliances such as cookers and space heaters. The same principle is also used in hydrogen sensors.

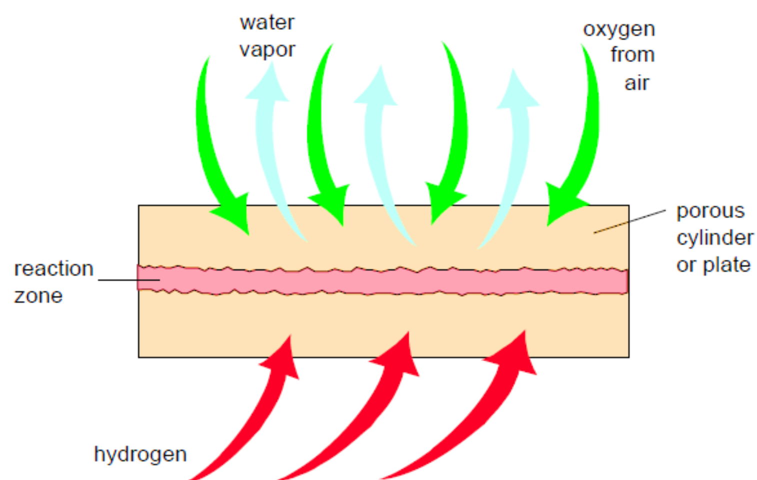

Fig.44 Schematic representation of catalytic burner..

Thinking of a practical application for hydrogen combustion (5), a good catalyst for the reaction of CHC should present high activity; it must work at low temperatures and work with a low flow of hydrogen. The metals that possess the right features are: Pt, Pd, Ir, Ru, Rh also Au and Ag. The only problem is the cost of these metals, to overcome this problem recent studies investigating on the use of more economic catalysts prepared as oxides: Co, Ni, Mn, Fe, Cr and Cu. They have a low catalytic ignition temperature but also a low-activity.

Platinum is a very well established catalyst and is one of the most active for CHC, capable of burning hydrogen even at room temperature [10-18].

The goal of this work is the dispersion of the noble metal (Pt) in the less expensive transition metal (Cu). Low hydrogen flow has been chosen to work. Increasing the temperature up to the transition metal activation temperature.

Catalyst should be prepared in supported form, which improves dispersion, prevents aggregation and facilitates it use in successive cycles. In the literature several types of material were screened for the search of inexpensive catalysts. Most papers report the use of metal oxides such as SiO_2, TiO_2, CeO_2, SnO_2, ZrO_2, etc and other ceramics as catalyst support [15, 19-21].

However, if CHC is thought to be employed for heating purposes, silicon carbide should be considered as a support of election due to its high mechanical strength, chemical inertness and high thermal conductivity to prevent the formation of hot spots [22]. SiC has been previously reported as a support for other catalytic reactions such as

methane (or methane/H_2 mixtures) combustion and Fischer–Tropsch reaction [22-27] but only recently for the CHC reaction [28, 30].

Given the high cost to limit the use of material, nanoparticle coatings have been chosen. When a thin film is deposited on a surface, it will form a new phase characterized by physical properties also very different from those in massive phase. The origin of these changes is in bond character of the thin layers in the microstructure and morphology of the layers. In the volume of a perfect crystal, the atoms are subject to binding forces in all directions, come from the neighboring atoms. However this does not happen in atoms from the surface. In this case there is symmetry in the directionality of the bonding forces, which makes the energy states of atoms on the surface are different from those of the interior. Because of this, many of the properties, physico-chemistry of surface atoms are also different [23].

The present work presents the study of this PtCu alloy on SiC foam as catalyst for CHC for very lean (1% v/v) H_2/air mixtures. This mixture is safe, and its hydrogen concentration allows to conduct the (very exothermic) reaction. For designing and controlling active catalysts, a fundamental understanding of the relationship between the activity and the surface electronic structure and surface chemistry is actively being pursued [30-35].

3.8- Catalytic test result

Conversion and temperature were monitored during the experiment and results are shown in Fig.45-46. The conversion vs temperature curves between the coatings under argon and helium gases, both as deposited and after 5' minutes of dealloying shows similar T_{50}.

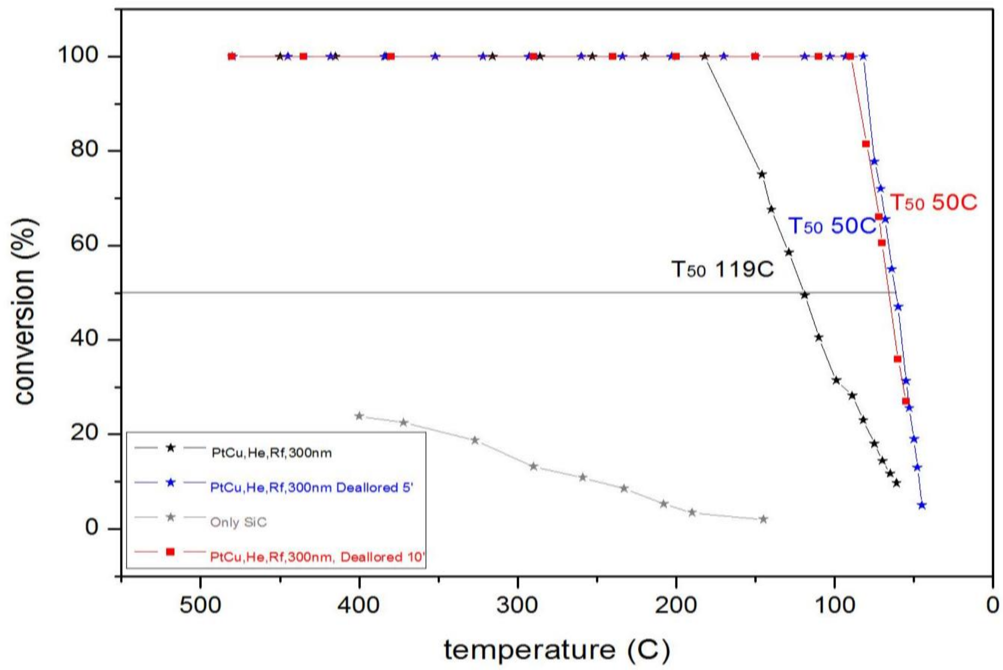

Fig.45 Conversion vs Temperature plot for coatings under Helium.

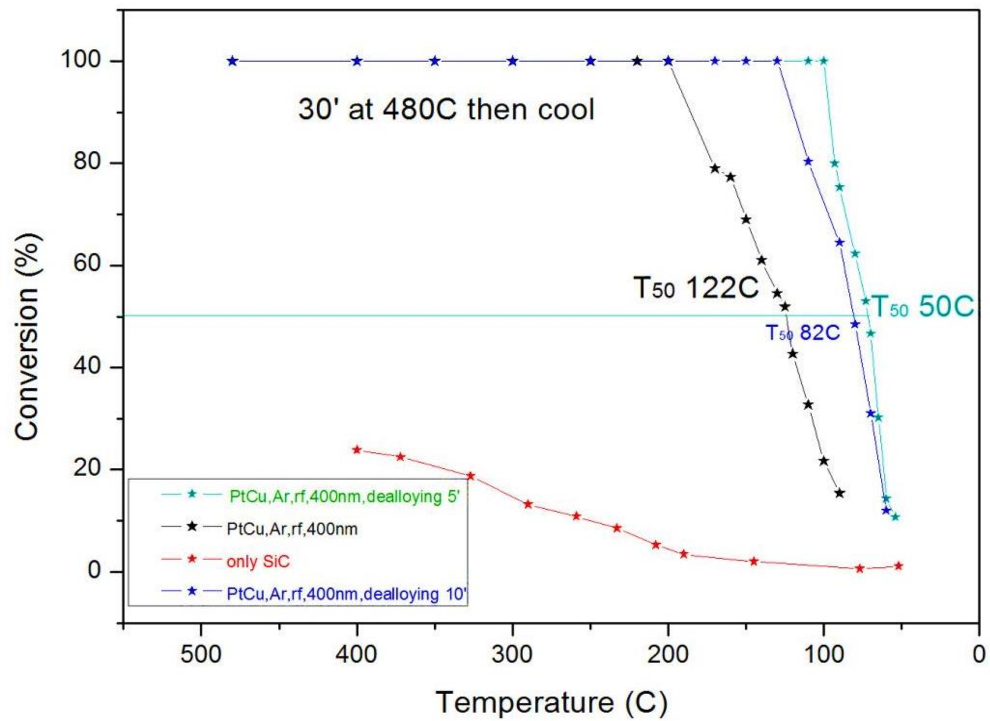

Fig.46 Conversion vs Temperature plot for coatings under Argon.

The activation energy, E_a, is the minimum energy molecules must possess in order to react to form a product. The E_a can be calculate using the Arrhenius equation

$$\boldsymbol{k = Ae^{-Ea/(RT)}} \qquad (6)$$

The slope of the Arrhenius plot can be used to find the activation energy. The Arrhenius plot Fig.47 is obtained by plotting the logarithm of the rate constant, k, versus the inverse temperature, 1/T.

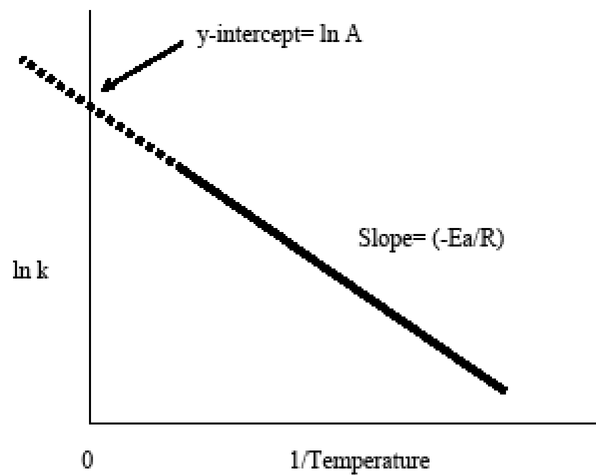

Fig.47 The Arrhenius plot.

The resulting negatively-sloped line is useful in finding the missing components of the Arrhenius equation. Extrapolation of the line back to the y-intercept yields the value for ln A. The slope of the line is equal to the negative activation energy divided by the gas constant, R. The Arrhenius equation $\ln k = -E_a/RT + lnA$ can be rearranged to deal with specific situations.

For example, taking the logarithm of both sides yields the equation above in the form y= mx+b. Then, plot ln k vs 1/T and all variables can be found.

The Arrhenius Plots are calculated for coatings as well as deposited and after treatment of dealloying. The results are shown in Fig.48-51 and in the Tab.4.

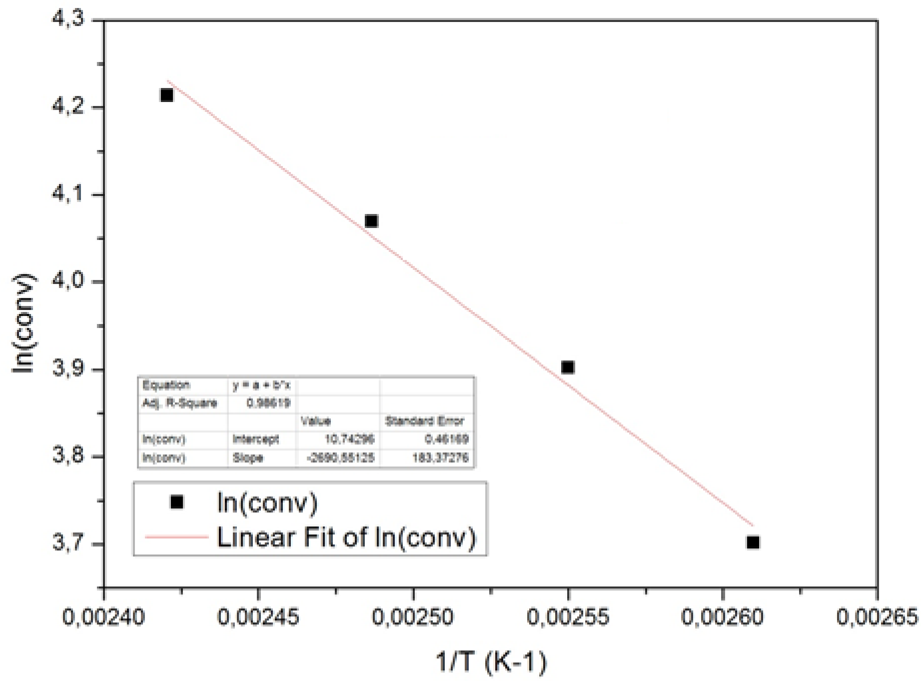

Fig.48 Arrhenius plot PtCu, He, 300 nm.

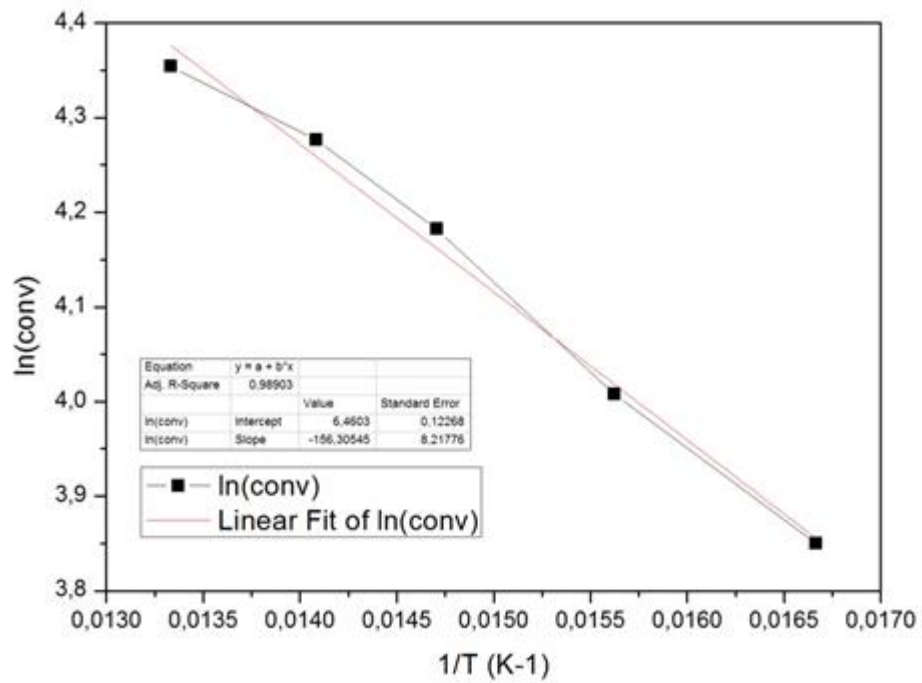

Fig.49 Arrhenius plot PtCu, He, 300 nm, dealloyed 5'.

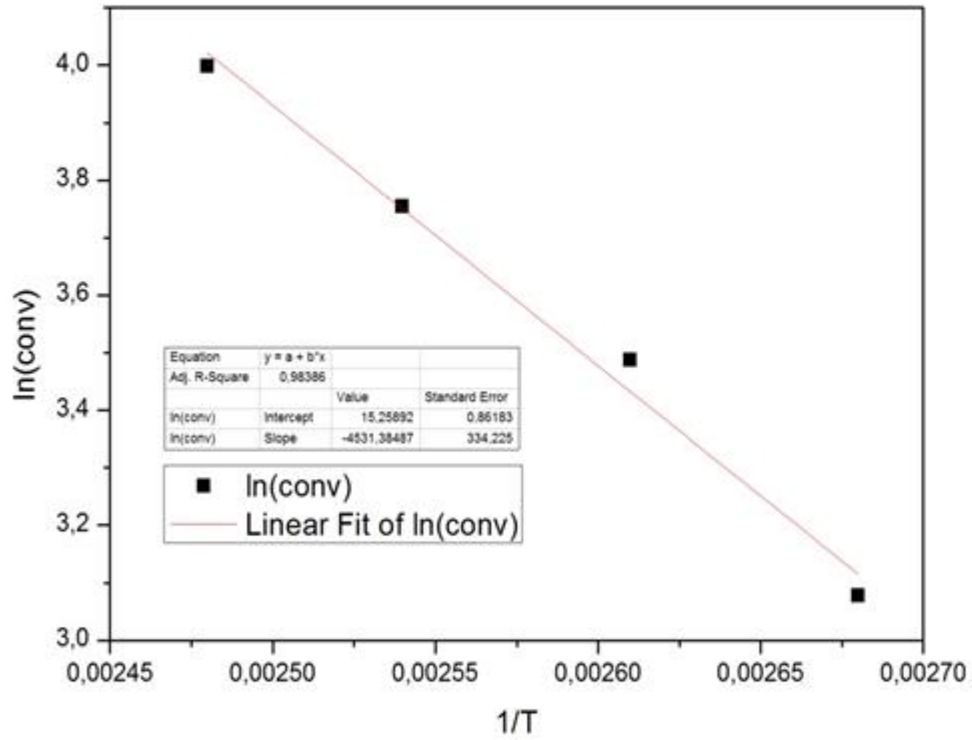

Fig.50 Arrhenius plot PtCu, Ar,400 nm.

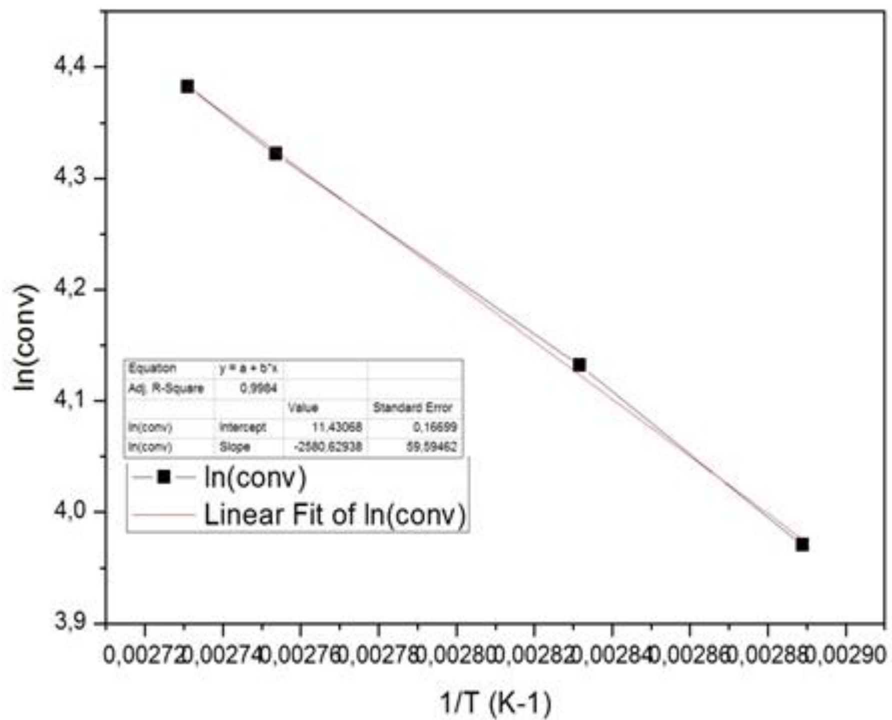

Fig.51 Arrhenius plot PtCu, Ar,400 nm, dealloyed 5'.

Tab.4- Energy of activation of the samples.

Sample	Ea (kJ/mol)
PtCu,He,RF,300nm	21±0,5
PtCu,He,RF,300nm,dealloyed 5’	1±0,1
PtCu,Ar,RF,400nm	38±0,9
PtCu,Ar,RF,400nm,dealloyed 5’	21±0,2

3.9-Conclusion

All the examined coatings follow the same trend their T_{50} drops markedly after treatment of dealloying, showing after 5’ of selective leaching the same value of T_{50} (50°C) for both types of coatings.

Same trend for the activation energy of the combustion reaction. The Arrhenius plots show the same behaviour for both films under argon and under helium. The coatings lower their activation energy after the dealloying process.

Coatings grown under helium, have lower activation energy as deposited and after dealloying, compared to the coatings under argon. This experimental evidence was connected to the marked difference in the morphology and porosity between the two alloys.

3.10–Experimental part

3.10.1-Synthesis of copper platinum alloys by magnetron sputtering and subsequent treatment of dealloying.

Before introducing the substrates into the chamber, they have undergone a cleaning treatment, just in order to eliminate possible organic and inorganic impurities, which involves:

- ultrasound treatment with milliQ®water at 80 °C during 15 minutes;
- then put under ultrasound with a mixture of 1:1 ethanol-acetone at room temperature during 15 minutes;
- then drying oven at 110°C, overnight.

After cleaning, the silicon carbide support has been inserted in the chamber of sputtering. The pumps were then switched on. The turbo-molecular pump is started once it reaches 10^{-3} mbar. At this point the heating of the substrate was started up at 70°C. No action was taken on the system for about 6 hours, at the end of which in the deposition chamber has reached a pressure of the order of 10^{-6}mbar. At this point is lowered to a suitable temperature up to 50°C, the system is left stationary for one hour and finally the heating is switched off. Reached the grade of vacuum, depending on the film to realize (Ar or He), gas was injected into the chamber sputtering, at a pressure of 4.8 10^{-2} mbar; this pressure is kept for the whole duration of the process. For the RF process, the following power value has been used: 100W.
The target in the first five minutes was covered, The sample holder is shown in Fig.52, it is rotating with the speed of 4 turns / min, to ensure greater to ensure the highest possible homogeneity. After completing these 5 minutes, the host cathode target was discovered and began the phase of cosputtering.

The duration of sputtering was set to achieve a comparable thickness of films. The times were selected to get close to 300/400 nm. The difference so marked in the times is clearly explained by the different speed of growth of the film under the two different gases. Tab.6 shows the coatings deposition condition.

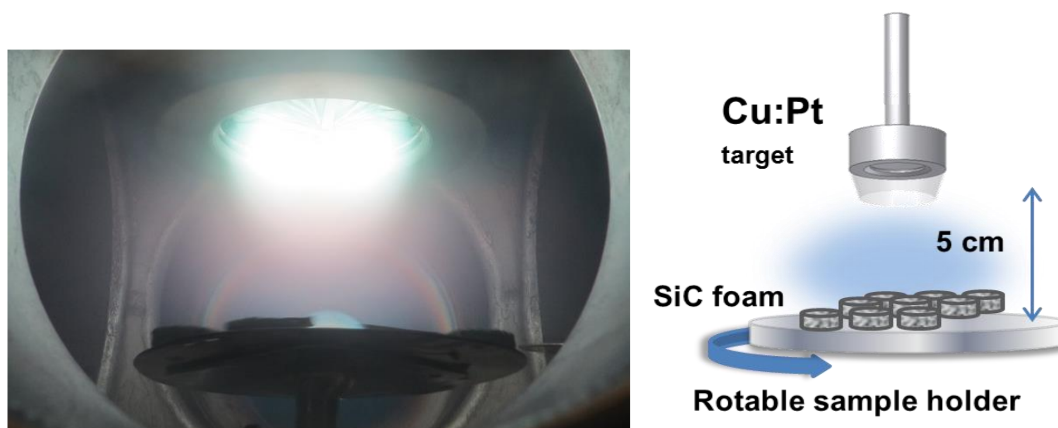

Fig.52 The magnetron sputtering chamber.

After the expiry of that time limit has been removed and the power supply has been interrupted the gas flow, through a suitable valve. It then proceeded with the shutdown of the turbo-molecular pump, which required a complete stop of about 70 minutes. After this time interval, the next step is switching off the rotary pump and with it also the cooling system. To be able to access the inside of the sputtering chamber, it is due to open an appropriate valve to allow air to enter, thus restoring the atmospheric pressure inside;.

Tab.5- Coatings deposition condition.

Sample	Target	Dep. gas	Power type	Power int. (W)	Pressure (mbar)	Dep. time (min)	Thickness (nm)	Dep. Rate (nm/min)
1	**PtCu**	**He**	**RF**	**100**	**4.8×10^{-2}**	**37,30’**	**300**	**8**
2	**PtCu**	**Ar**	**RF**	**100**	**4.8×10^{-2}**	**7,30’**	**400**	**55**

The dealloying of the Pt-Cu films was carried out in 65% concentrated nitric acid 14,4 M at room temperature. When achieving the desired etching time, the samples are then immersed in distilled water for several minutes to stop the dealloying process and remove the residue acid nitric. Before being characterized coatings are dried in an oven

for one hour at 110°C. After dealloying, most Cu is removed from the surface and partially from the interior, leaving a nearly pure Pt enriched surface layer. Tab.6 shows time of selective leaching for the samples.

Tab.6- Dealloying time.

Sample	Target	Depositon gas	Dealloying time
1	**PtCu**	**He**	**5'-10'**
2	**PtCu**	**Ar**	**5'-10'**

3.10.2- Support and catalyst characterization SEM

Plan-view and cross-section SEM characterization analyses were performed on the as prepared support and catalyst in a high resolution SEM-FEG microscope Hitachi S4800 operating at 5 keV. The chemical composition was determined by EDX detector (Bruker-X Flash-4010) it allows the registration of individual elemental mapping. Quantification of EDX spectra was done with the Expirit 1.8 software from Bruker. For the structural analysis of the films, XRD (X-ray Diffraction) measurements were performed on Si(100) and powdery material using the Cu Kα radiation in a Siemens D5000 diffractometer in a Bragg-Brentano configuration in the 38°÷54° 2θ angle range.

3.10.3- Catalytic test

Catalytic tests were executed in a fixed bed reactor connected to a gas chromatograph to detect the combustion reaction product: the water. The catalyst in monolithic form was loaded into the reactor in contact with a bed of quartz and in contact with a thermocouple. The reaction is performed in a poor atmosphere of hydrogen only 1% v/v H_2 in air. The system is calibrated by measuring a chromatogram at room temperature with the oven turned off.

The reaction is conducted up to 480 degrees, after half an hour at this temperature the system is cooled and were recorded the data necessary to measure the activity (T_{50} and energy of activation). The heat released by the reaction would be negligible in the very lean H_2/air mixtures and thus the formation of hot spots should not be an issue here.

The conversion is calculated by comparing the peak of hydrogen at a temperature (x) with the hydrogen peak of the blank. Water was therefore detected as vapor into the exhaust gases by measuring the intensity of peaks of hydrogen and oxygen with a gas chromatograph. The reactor was heated from out-side using an electric furnace and temperature was controlled using a PID controller. Temperature was measured by a K-type thermocouple placed at the center of the fixed bed reactor. The representation of equipment used is shown in Fig.53.

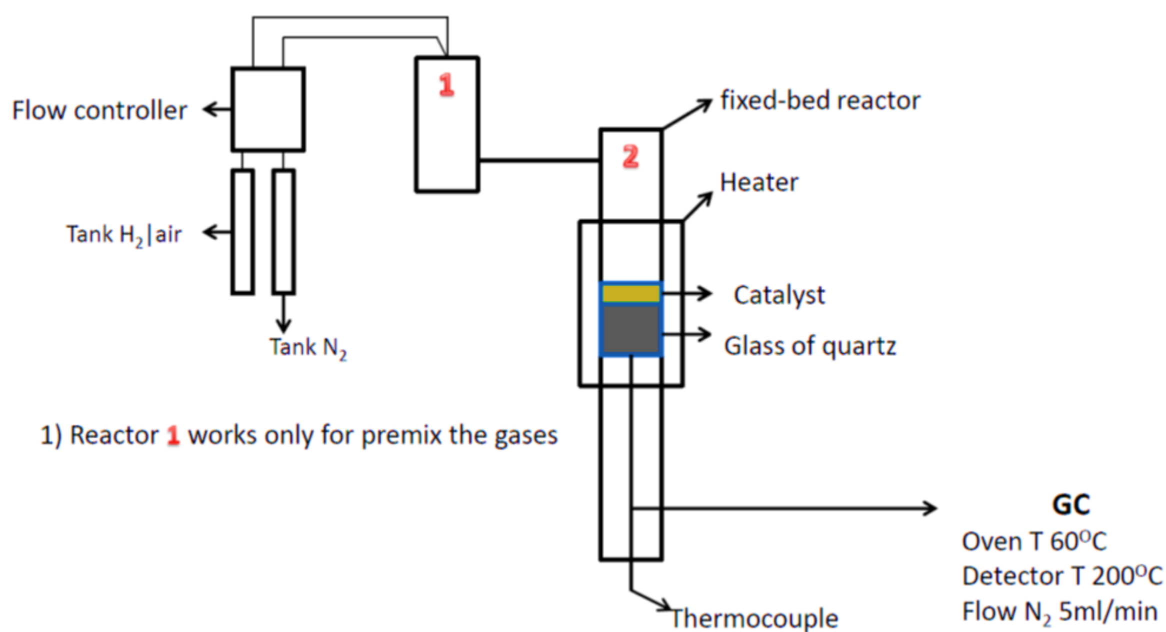

Fig.53 Representation system used.

Catalyst was tested with no previous conditioning treatment. The methodology of measuring water through GC method. For this purpose, an Agilent Technologies 7890B chromatograph system was employed to measure H_2 amount, with an Agilent J&W GC capillary columns and a thermal conductivity detector. N_2 was used as a carrier gas. The PtCu coatings were characterized by a kinetic point of view; all the analyzed samples were analyzed under the same experimental conditions (H_2 concentration, mixture flow rate).

The CHC was studied at 480 °C using a flow of 1% v/v of H_2/air mixture. The conversion vs. temperature curve for the PtCu coating on SiC foam was measured in cooling mode from 480 °C to room temperature. The reactor temperature was first set at 480°C and was left at this temperature for 30’ minutes to ensure the homogeneity

throughout the reaction zone, then left to cool to room temperature with the aid of the electric oven.

4 –CONCLUSIONS

- The Magnetron sputtering methodology has been proved adequate for the fabrication of Pt-Cu catalytic coatings. The methodology of introducing a He plasma is presented here as the first time for the fabrication of porous catalytic coatings. For pratical purposes a single target arrangement was used which reduces the consumption of platinum.
    - The porous PtCu films where deposited on porous SiC foam showing *good adhesion* for undertaken dealloying procedures and the activity measurements.
    - The dealloying procedure is bringing a new class of nanoporous catalysts in which the particle size reduction (or the noble metal dispersion) seems to be one factor for incresing catalytic activity. The other examined in this thesis is the type of porosity.
    - The production of nanoporous platinum through the selective dissolution at room temperature of Cu from Pt has been demonstrated. The characterization by means of SEM microscopy and EDX analysis confirm the presence of porous with a diameter of approximately 4-21 nm. The small size was attributed to the extremely small values of surface diffusivity expected for platinum at room temperature. The ease of production of porous platinum may make this method of processing attractive for applications as high surface area biomedical electrodes or as catalyst materials.
- The PtCu supported catalysts, before and after the dealloying procedure, were tested for the first time in the catalytic hydrogen combustion reaction.
    - The T_{50} temperature was strongly reduced as well as the combustion activation energy. The results are very promising for the reaction working spontaneously above 0 ºC.
    - Our results show that dealloyed PtCu thin films consisting of a Pt enriched surface layers are overall more strained and enriched than the as deposited films. These effects dominate the CHC activity enhancement of the dealloyed films.

References

1. https://ec.europa.eu/programmes/horizon2020/en/area/key-enabling-technologies#Article
2. http://www.nanotechproject.org/topics/nano101/introduction_to_nanotechnology/
3. Mattox, D.M., *Handbook of Physical Vapor Deposition (PVD) Processing*. Handbook of Physical Vapor Deposition (PVD) Processing. 2010.
4. Depla, D., S. Mahieu, and J.E. Greene, *Sputter Deposition Processes*, in *Handbook of Deposition Technologies for Films and Coatings*. 2010. p. 253-296.
5. Sproul, W.D., D.J. Christie, and D.C. Carter, *Control of reactive sputtering processes.* Thin Solid Films, 2005. **491**(1-2): p. 1-17.
6. Artymowicz, D.M., J. Erlebacher, and R.C. Newman, *Relationship between the parting limit for de-alloying and a particular geometric high-density site percolation threshold.* Philosophical Magazine, 2009. **89**(21): p. 1663-1693.
7. Schuppert, A.K., et al., *Composition-Dependent Oxygen Reduction Activity and Stability of Pt-Cu Thin Films.* ChemElectroChem, 2014. **1**(2): p. 358-361.
8. Pugh, D.V., A. Dursun, and S.G. Corcoran, *Formation of nanoporous platinum by selective dissolution of Cu from Cu0.75Pt0.25.* Journal of Materials Research, 2003. **18**(1): p. 216-221.
9. Tomašić, V. and F. Jović, *State-of-the-art in the monolithic catalysts/reactors.* Applied Catalysis A: General, 2006. **311**: p. 112-121.
10. Haruta, M. and H. Sano, *Catalytic combustion of hydrogen—IV. Fabrication of prototype catalytic heaters and their operating properties.* International Journal of Hydrogen Energy, 1982. **7**(10): p. 801-807.
11. Deshpande, P.A. and G. Madras, *Catalytic hydrogen combustion for treatment of combustible gases from fuel cell processors.* Applied Catalysis B: Environmental, 2010. **100**(3–4): p. 481-490.
12. Haruta, M. and H. Sano, *Catalytic combustion of hydrogen I—Its role in hydrogen utilization system and screening of catalyst materials.* International Journal of Hydrogen Energy, 1981. **6**(6): p. 601-608.
13. Haruta, M., Y. Souma, and H. Sano, *Catalytic combustion of hydrogen—II. An experimental investigation of fundamental conditions for burner design.* International Journal of Hydrogen Energy, 1982. **7**(9): p. 729-736.
14. Wierzba, I. and A. Depiak, *Catalytic oxidation of lean homogeneous mixtures of hydrogen/hydrogen–methane in air.* International Journal of Hydrogen Energy, 2004. **29**(12): p. 1303-1307.
15. Choi, W., S. Kwon, and H. Dong Shin, *Combustion characteristics of hydrogen–air premixed gas in a sub-millimeter scale catalytic combustor.* International Journal of Hydrogen Energy, 2008. **33**(9): p. 2400-2408.
16. Morfin, F., J.-C. Sabroux, and A. Renouprez, *Catalytic combustion of hydrogen for mitigating hydrogen risk in case of a severe accident in a nuclear power plant: study of catalysts poisoning in a representative atmosphere.* Applied Catalysis B: Environmental, 2004. **47**(1): p. 47-58.

17. Sanap, K.K., et al., *Supported Pt nanoparticles for the hydrogen mitigation application.* International Journal of Hydrogen Energy, 2014. **39**(27): p. 15142-15155.
18. Deshpande, P.A. and G. Madras, *Noble metal ionic sites for catalytichydrogen combustion: spectroscopic insights.* Physical Chemistry Chemical Physics, 2011. **13**(2): p. 708-718.
19. Zhang, C., J. Zhang, and J. Ma, *Hydrogen catalytic combustion over a Pt/Ce0.6Zr0.4O2/MgAl2O4 mesoporous coating monolithic catalyst.* International Journal of Hydrogen Energy, 2012. **37**(17): p. 12941-12946.
20. 11. Shinde, V.M. and G. Madras, *Kinetic studies of ionic substituted copper catalysts for catalytic hydrogen combustion.* Catalysis Today, 2012. **198**(1): p. 270-279.
21. Hanson, F.V. and M. Boudart, *The reaction between H2 and O2 over supported platinum catalysts.* Journal of Catalysis, 1978. **53**(1): p. 56-67.
22. Marín, P., S. Ordóñez, and F.V. Díez, *Performance of silicon-carbide foams as supports for Pd-based methane combustion catalysts.* Journal of Chemical Technology & Biotechnology, 2012. **87**(3): p. 360-367.
23. Guo, X., et al., *Structural evolution of plasma-sputtered core-shell nanoparticles for catalytic combustion of methane.* Journal of Physical Chemistry C, 2011. **115**(49): p. 24164-24171.
24. Leroi, P., et al., *Ni/SiC: a stable and active catalyst for catalytic partial oxidation of methane.* Catalysis Today, 2004. **91–92**: p. 53-58.
25. De Tymowski, B., et al., *Co–Ru/SiC impregnated with ethanol as an effective catalyst for the Fischer–Tropsch synthesis.* Applied Catalysis A: General, 2012. **419–420**: p. 31-40.
26. Specchia, S., S. Tacchino, and V. Specchia, *Facing the catalytic combustion of CH4/H2 mixtures into monoliths.* Chemical Engineering Journal, 2011. **167**(2–3): p. 622-633.
27. Tacchino, S., L.D. Vella, and S. Specchia, *Catalytic combustion of CH4 and H2 into micro-monoliths.* Catalysis Today, 2010. **157**(1–4): p. 440-445.
28. Godinho, V., T.C. Rojas, and A. Fernandez, *Magnetron sputtered a-SiOxNy thin films: A closed porous nanostructure with controlled optical and mechanical properties.* Microporous and Mesoporous Materials, 2012. **149**(1): p. 142-146.
29. Godinho, V., et al., *Microstructural characterization of hydrophobic Ti1−xAlxN coatings with moth-eye-like surface morphology.* Journal of Alloys and Compounds, 2012. **536, Supplement 1**: p. S398-S406.
30. Mukerjee, S., et al., *Role of structural and electronic properties of Pt and Pt alloys on electrocatalysis of oxygen reduction an in situ XANES and EXAFS investigation.* Journal of The Electrochemical Society, 1995. **142**(5): p. 1409-1422.
31. Marković, N.M. and P.N. Ross Jr, *Surface science studies of model fuel cell electrocatalysts.* Surface Science Reports, 2002. **45**(4–6): p. 117-229.
32. Nørskov, J.K., et al., *Origin of the Overpotential for Oxygen Reduction at a Fuel-Cell Cathode.* The Journal of Physical Chemistry B, 2004. **108**(46): p. 17886-17892.
33. Stamenkovic, V., et al., *Changing the Activity of Electrocatalysts for Oxygen Reduction by Tuning the Surface Electronic Structure.* Angewandte Chemie (International Edition), 2006. **45**(18): p. 2815.

34. Greeley, J. and J.K. Nørskov, *Combinatorial Density Functional Theory-Based Screening of Surface Alloys for the Oxygen Reduction Reaction.* The Journal of Physical Chemistry C, 2009. **113**(12): p. 4932-4939.
35. Greeley, J., et al., *Alloys of platinum and early transition metals as oxygen reduction electrocatalysts.* Nature Chemistry, 2009. **1**(7): p. 552-556.